Quaternary Science Reviews xxx (xxxx) 110036

Contents lists available at ScienceDirect

Quaternary Science Reviews

journal homepage: www.elsevier.com/locate/quascirev

# Precise dating of the 686 ± 2 CE Newberry Pumice eruption and insights into 7th century volcanism from cryptotephra and sulfur isotopes in Greenland ice

Helen M. Innes[a,*], William Hutchison[a], Michael Sigl[b], Joseph R. McConnell[c], Nathan J. Chellman[c], Britta J.L. Jensen[d], Jakub T. Sliwinski[a], Andrea Burke[a]

[a] Univeristy of St Andrews, UK
[b] University of Bern, Switzerland
[c] Desert Research Institute, NV, USA
[d] University of Alberta, Edmonton, Canada



A B S T R A C T

Greenland ice core sulfate records reveal several large-magnitude volcanic events during the 7th Century of the Common Era (CE). The largest eruptions, in 626 and 682 CE, coincide with negative tree ring growth anomalies and documented evidence of climate cooling and societal crises. However, their volcanic sources remain unidentified, leaving major uncertainties about eruption latitude, sulfur injection height and climate forcing potential. Here, we analyse sulfur isotopes of deposited sulfate aerosol and cryptotephra geochemistry in Greenland ice core Tunu2013 to better constrain eruptive sources for the 626 and 682 CE eruptions, and additionally, a sulfate peak at 698 CE and a tephra deposit at 686. We present the first identification of the Newberry Pumice tephra in Greenland ice (686 ± 2 CE), extending the known spatial distribution of this North American tephrostratigraphic marker. Sulfur isotope data indicates this Newberry eruption injected sulfur primarily into the troposphere, consistent with previous studies. Isotopic evidence confirms that the 626 and 682 CE eruptions had stratospheric plume heights and were from extratropical Northern Hemisphere and tropical sources, respectively. The 698 CE sulfate peak is revised from an assumed tropical eruption, to a tropospheric, extratropical Northern Hemisphere eruption. Although cryptotephra geochemistry does not conclusively match known volcanic events, shards coincident with the 626 CE peak suggest an unidentified North Pacific arc source. Recurrent rhyolitic tephra throughout our sample set may reflect pulses of Southern Mono Craters activity, multiple unrelated volcanic events, or secondary remobilisation and deposition. These results demonstrate the value of integrating sulfur isotope and tephra analyses to refine reconstructions of volcanic–climate linkages.

## 1. Introduction

Stratospheric sulfur emissions following large volcanic eruptions can cause regional and global cooling lasting several years and make volcanoes one of the most important drivers of natural climate variability (Cole-Dai, 2010; Robock, 2000). The climate response following volcanic eruptions is sensitive to key source parameters such as plume height, source location, sulfur loading and season of eruption (Marshall et al., 2019; Toohey et al., 2011, 2019). To better inform climate model simulations and predictions of volcanic impacts on global climate and society, it is important that these parameters are well constrained (Jungclaus et al., 2017).

Polar ice cores preserve the most complete record of past volcanic eruptions. These archives can be used to constrain key eruption parameters of interest when understanding climate response to volcanism. Volcanic events are usually preserved as peaks in sulfate and particle concentration (volcanic ash), and the former can be used to estimate sulfate loading and radiative forcing for past events (Cole-Dai, 2010; Gao et al., 2008; Plunkett et al., 2023; Toohey and Sigl, 2017). However, the majority of volcanic sulfate signals preserved in ice cores are yet to be linked to known volcanic sources, requiring major assumptions about their source latitude, plume height, and stratospheric sulfate loading. Recent studies have demonstrated that these parameters strongly influence volcanic radiative forcing and climate response (Burke et al., 2023; Marshall et al., 2019, 2022; Stevenson et al., 2017; Toohey et al., 2019) making efforts to extract new information from the volcanic ice core record of key importance for climate modelling and global preparedness for future, large-magnitude events.

Developments in S isotope analysis of ice core sulfate provide valuable constraints on eruption plume height and source latitude (Burke et al., 2019, 2023; Gautier et al., 2019). Sulfur injected in and above the ozone layer by explosive volcanism is exposed to UV radiation, imparting

* Corresponding author.
*E-mail address:* hi7@st-andrews.ac.uk (H.M. Innes).

https://doi.org/10.1016/j.quascirev.2026.110036
Received 3 November 2025; Received in revised form 23 April 2026; Accepted 28 April 2026
0277-3791/

a mass-independent isotopic anomaly (via photochemical reactions) that is preserved in sulfate deposited at the poles and can ultimately then be measured in ice cores (Baroni et al., 2007; Burke et al., 2019; Savarino et al., 2003). Sulfur isotopes of volcanic sulfate in ice cores not only provide important constraints on plume heights, but also source location (latitude). This is because fallout from tropical eruptions deposited in the polar regions consists exclusively of stratospheric mass-independent fractionated (MIF) sulfur whereas fallout from extratropical eruptions usually involves mixture of stratospheric (MIF) and tropospheric (non-MIF) sulfur due to closer proximity to the ice sheet (Burke et al., 2019, 2023). Geochemical fingerprinting of tephra glass remains the only robust way to link an ice core deposit with its specific eruptive source (e.g. Abbott et al., 2024; Davies et al., 2024; Lowe, 2011; Plunkett et al., 2023). Together, these two techniques provide a powerful framework for identifying and characterising specific volcanic eruptions in ice cores (Hutchison et al., 2025; Pearson et al., 2022), which can be particularly important when assessing volcano-climate forcing for events associated with major temperature perturbations.

During the 7th Century of the Common Era (600-700 CE), a number of large magnitude volcanic events are identified as sulfate peaks in polar ice cores (Fig. 1), none of which have a confirmed volcanic source (Gao et al., 2016; Plunkett et al., 2023; Sigl et al., 2015; Toohey and Sigl, 2017). Of particular note are the two largest volcanic sulfate peaks of the century, which are deposited in Greenland starting in 626 CE and 682 CE and are linked to Northern Hemisphere cooling shown by tree ring width and maximum latewood density temperature reconstructions (Büntgen et al., 2016, 2025; Gao et al., 2016; Salzer and Hughes, 2007; Schneider et al., 2015; Sigl et al., 2015). Sulfate deposits from the 626 CE eruption are only found in Greenland ice cores (Fig. 1), suggesting an extratropical latitude Northern Hemisphere source (Sigl et al., 2015). This is further supported by sulfur isotope analysis of the ice core eruption deposit which provides evidence for a Northern Hemisphere, extratropical, stratospheric eruption (Burke et al., 2023). Of all ice core-recorded eruptions of the last 2000 years, the Northern Hemisphere extratropical temperature response linked with the 626 CE eruption is ranked as the second largest (Büntgen et al., 2025), and frost ring signals and ring width minima occur in North American bristlecone pines in 627 CE (Salzer and Hughes, 2007). Historical eyewitness accounts of dry fogs and dimming of the Sun in the Mediterranean region during 626 and 627 CE support stratospheric volcanic aerosol injection in 626 CE (Stothers, 2002; Stothers and Rampino, 1983), and volcanic induced cooling has been suggested as an environmental factor for driving documented societal disruption including population migration and the fall of the Turkic empire (Büntgen et al., 2016; Di Cosmo et al., 2017; Fei et al., 2007). The 682 CE event is thought to be a tropical eruption due to its bipolar sulfate deposits (Sigl et al., 2015) and the presence of stratospheric sulfur in Antarctic ice (Gautier et al., 2019). The 682 CE volcanic stratospheric sulfur injection (VSSI) of 27.2 Tg S is ranked as the 7th largest of the last 2500 years (Toohey and Sigl, 2017), with spatially varying Northern Hemisphere tree ring minima and societal stresses following the hypothesised tropical eruption (Gao et al., 2016).

To date, no volcanic sources have been identified for the eruptions in 626 and 682 CE or any other eruptions of the 7th Century which have been recorded in polar ice cores (Plunkett et al., 2023). From radiocarbon dating of proximal ash deposits, it has been hypothesised that major VEI 5-6 (Volcanic Explosivity Index; Newhall and Self, 1982) eruptions of Rabaul, Witori, and Dakataua from New Britain Island are candidates for the 682 CE tropical eruption (Gao et al., 2016; McKee et al., 2011; Sigl et al., 2015). Radiocarbon wiggle-match dating of the Rabaul Pyroclastics eruption to 667-699 CE has led to the suggestion it is the most likely candidate for the 682 CE eruption (McKee et al., 2015). Additional ≥ VEI 4 eruptions (considered to be the minimum VEI required to transport ash to Greenland; Plunkett et al., 2022) within dating uncertainty of the 7th Century ice core sulfate peaks are listed in eruption databases LaMEVE (Crosweller et al., 2012) and the Global Volcanism Project (https://volcano.si.edu/),representing plausible candidates for the major 7th Century ice core sulfate peaks (Table 1). For the 626 CE eruption, prominent Northern Hemisphere eruptions candidates include the Kamchatka volcanoes Opala (Baranii Amphitheatre eruption; VEI 6) (Andrews et al., 2018; Plunkett et al., 2015; Ponomareva et al., 2017) and Shiveluch (eruptions SH#9 to SH#12; VEI 4-5) (Plunkett et al., 2015), and North American eruptions of Newberry (Newberry Pumice eruption; VEI 4) (Jensen et al., 2021; Kuehn, 2002; Kuehn and Foit, 2006) and Southern Mono Craters (the penultimate Mono Craters eruption; VEI 4) (Bursik et al., 2014; Jensen et al., 2021). These Northern Hemisphere eruptions are all radiocarbon dated to within uncertainty of the extratropical 626 CE eruption (see Table 1 for details) and are known to have produced eruptions with widespread tephra trans-

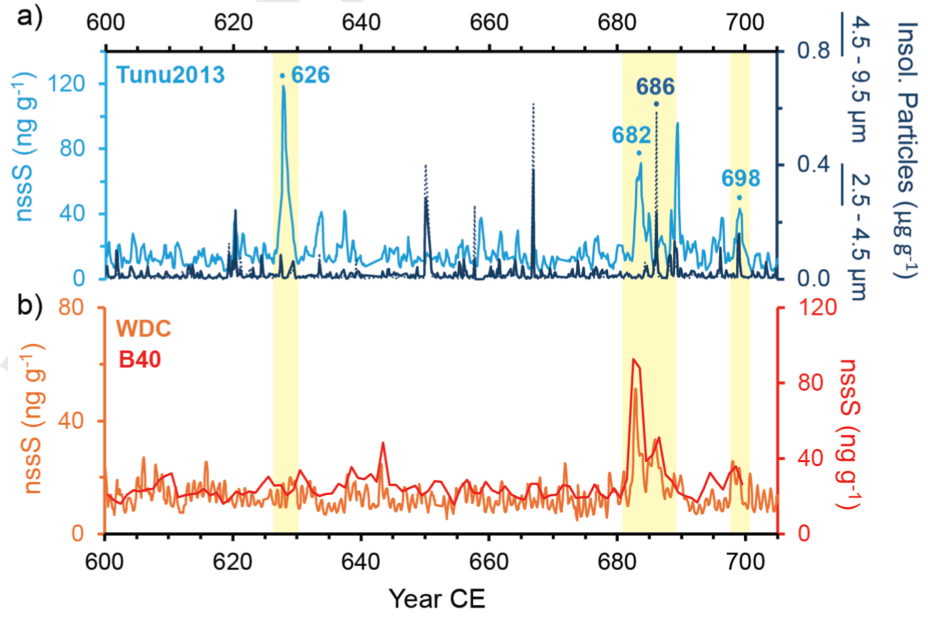


**Fig. 1.** Continuous nssS (non-sea salt sulfur) records from Greenland ice core Tunu2013 and Antarctic ice cores WDC and B40 (Sigl et al., 2015), and insoluble particle data from Greenland identifying key volcanic sulfur peaks across the 7th Century Common Era (CE). Events sampled in 626, 682, 686 and 698 CE from Tunu2013 ice core are labelled and highlighted yellow.

**Table 1**
Candidate eruptions for 7th Century eruptions preserved in Greenland ice as listed in the LaMEVE database (Crosweller et al., 2012) or suggested by previous studies discussing Greenland sulfate peaks during this period (Gao et al., 2016; McKee et al., 2015; Sigl et al., 2015; Zielinski et al., 1994).

| Candidate Source *and Eruption* | Region | Reported Eruption Date (CE) | VEI | Geochemistry | Latitude |
|---|---|---|---|---|---|
| **Arenal** *Et-7* | Costa Rica | ~650 (Bolge et al., 2006) | 4 | Andesite-Dacite (Bolge et al., 2006) | Tropical |
| **Bezymianny** | Kamchatka, Russia | 700 ± 50 CE Suggested as candidates by (Gao et al., 2016; Zielinski et al., 1994) | 4 | Andesite? (Ponomareva et al., 2017) | Northern Hemisphere |
| **Cotopaxi** *L1* | Ecuador | ~740 (Barberi et al., 1995; Hall and Mothes, 2008) | 4 | Andesite ((Garrison et al., 2011); not specific eruption) | Tropical |
| **Dakataua** *Dk* | New Britain Island, Papua New Guinea | 605-675 (McKee et al., 2011) | 6 | Andesite-Dacite (Firth et al., 2024; Neall et al., 2021) | Tropical |
| **El Chichon** *D* | Mexico | ~700 (Espíndola et al., 2000) | ≤5? | Trachyandesite (No data for D, (Nooren et al., 2017) for E). | Tropical |
| **Furnas** *E* | Azores | ~600 (Cole et al., 1999) | 4 | Trachyte (Wastegård et al., 2020) | Northern Hemisphere |
| **Miyakejima** *Suoana-Kazahava* | Japan | 600 ± 54 (Geshi et al., 2022) | 4 | Basalt-Andesite (Geshi et al., 2022); whole rock) | Northern Hemisphere |
| **Newberry** *Newberry Pumice* | Oregon, USA | 635 ± 70 (Jensen et al., 2021) | 4 | Rhyolite (Jensen et al., 2021) | Northern Hemisphere |
| **Opala** *Baranii Amphitheatre* | Kamchatka, Russia | 550-635 (Braitseva et al., 1995, 1997) | 6 | Rhyolite (Andrews et al., 2018; Plunkett et al., 2015; Portnyagin et al., 2020) | Northern Hemisphere |
| **Witori** *WK-4* | New Britain Island, Papua New Guinea | 620-780 (McKee et al., 2011) | 5 | Dacite (Firth et al., 2024; Neall et al., 2021) | Tropical |
| **Rabaul** *Rabaul Pyroclastics* | New Britain Island, Papua New Guinea | 667-699 (McKee et al., 2015) | 6 | Dacite (Fabbro et al., 2020) | Tropical |
| **Sete Cidades** *P15- P12 (LaMEVE)* | Azores | ~528-1039 (770 mean) (Moore and Rubin, 1991; Queiroz et al., 2008) | 4 | Trachyte (Ellis et al., 2023; Queiroz et al., 2015) | Northern Hemisphere |
| **Shiveluch** *SH#9 – SH#12* | Kamchatka, Russia | ~470-800 (Ponomareva et al., 2015) | 4-5 | Andesite – Rhyolite (Ponomareva et al., 2015; Portnyagin et al., 2020) | Northern Hemisphere |
| **Southern Mono Craters** | California, USA | 600-650 CE (Bursik et al., 2014; Jensen et al., 2021) | 4 | Rhyolite (Jensen et al., 2021) | Northern Hemisphere |

port. Confirming any of these candidates as sources for ice core sulfate deposits requires identification and geochemical correlation of primary deposits of tephra or cryptotephras (microscopic, non-visible tephra) in ice.

Here, we combine high-resolution sulfur isotope analysis and tephra geochemical characterisation to interpret eruptive characteristics of prominent 7th Century eruptions recorded in a Greenland ice core. We specifically target events in 626 and 682 CE which have the greatest VSSI of the 7th Century (Toohey and Sigl, 2017) and are associated with Northern Hemisphere climate cooling. In addition to these two notable events, we use these methods to investigate a further hypothesised tropical eruption deposited as a sulfate peak at 698 CE and a peak in particle concentration associated with a small sulfate increase during 686 CE (Fig. 1). Using these methods, we provide new constraints on the source, timing and plume height of four major eruptions of the 7th Century and establish valuable new Northern Hemisphere tephra isochrons.

## 2. Methods

### 2.1. Ice core sampling

The Tunu2013 ice core (78° 2.1′ N, 33° 52.8’ W, 2105 m; 213 m total depth (Sigl et al., 2015) has previously been analysed using the high-resolution continuous flow analysis (CFA) system at the Desert Research Institute (DRI; Reno, NV) for a broad range of chemical and elemental species, including total sulfur concentration determined by inductively coupled plasma mass spectrometry and size-resolved insoluble particle concentrations determined by a laser-based particle detector (McConnell et al., 2002; Sigl et al., 2015) (Fig. 1). The core was dated using volcanically synchronized annual layer counting (Sigl et al., 2015).

This study targets the largest volcanic sulfate deposits in Greenland ice cores during the 7th Century which are associated with major Northern Hemisphere climate forcing, preserved as peaks in sulfate concentration in Tunu2013 beginning at 626 and 682 CE (Fig. 1). The decade 680-690 CE contains multiple sulfate peaks (682-686 CE, 689-690 CE) along with a prominent peak in medium (2.6–4.5 μm) and large (4.5–9.5 μm) insoluble particles at 686 CE. Therefore, this whole 680-690 CE interval, which includes the targeted 682 CE eruption, was selected for sampling. However, discrete sample analysis shows that the 689-690 CE sulfate peak was not fully captured and therefore it is not included in our study. In addition to climatically significant eruptions in 626 and 682 CE, a previously assumed tropical eruption at 698 CE was also sampled.

For sulfur isotope and tephra analysis, ice corresponding to each of the targeted ice core sections was discretely sub-sampled at intervals of 3–4 cm, equating to approximately 3 samples per year. Additional 5 cm samples were taken prior to the sulfate peaks to constrain background sulfate concentration in ice unaffected by large volcanic events. A total of 13 samples were cut for the 626 CE eruption across the depth interval 173.68–173.19 m, and 8 samples for the 698 CE eruption from 165.88 to 165.63 m. A continuous section was cut from depth interval 167.86–166.92 m to include the targeted tropical sulfate peak from the 682 CE event, additional peaks in sulfate 680-690 CE, and the particle peak at 686 CE comprising 30 individual samples.

### 2.2. Sulfur isotopes

Sulfate concentration of meltwater samples was measured by ion chromatography using a Metrohm 930 compact IC flex at the University of St Andrews. Samples were then centrifuged at 3000 rpm for 15 min and supernatant water pipetted off for sulfur isotope analysis, leaving $<5$ ml meltwater containing tephra and dust particles.

Following ion chromatography, a portion of each sample containing 20 nmol of $SO_4$ was dried down at 104 °C. Sulfate was isolated for isotopic analysis using anion exchange column chemistry (Burke et al., 2019) alongside an in-house secondary standard, Switzer Falls river water (Burke et al., 2018), and a procedural blank in each column set. Triple sulfur isotopes ($^{32}S$, $^{33}S$ and $^{34}S$) were measured using a Neptune Plus multi-collector inductively coupled plasma mass spectrometer (MC-ICP-MS) at the University of St Andrews Isotope Geochemistry laboratory (STAiG). Following isotopic analysis, $\delta^{34}S$, $\delta^{33}S$ and $\Delta^{33}S$ were

calculated using the equations:

$$\delta^X S = \left({}^X S / {}^{32} S\right)_{Sample} \Big/ \left({}^X S / {}^{32} S\right)_{Reference} - 1 \quad (1)$$

and

$$\Delta^{33} S = \delta^{33} S - \left(\left(\delta^{34} S + 1\right)^{0.515} - 1\right) \quad (2)$$

where $X$ is 33 or 34, and $\Delta^{33}$S is the measure of sulfur mass independent isotopic fractionation (S-MIF) of the sulfur deposited. Note when written with per mil units (‰), the above equations are multiplied by 1000. Isotopic values reported are relative to the Vienna-Canyon Diablo Troilite (V-CDT) reference standard. Mass dependent sulfur which remains below the ozone layer in the troposphere carries a $\Delta^{33}$S within analytical uncertainty of 0 ‰. Mass independently fractionated S carries a non-zero $\Delta^{33}$S anomaly due to photochemical reactions during exposure to UV radiation above the ozone layer (Savarino et al., 2003). The Switzer Falls secondary standard has a measured composition of $\delta^{34}S = 4.17 \pm 0.11$ ‰ (2 σ) (Burke et al., 2018). Over the course of this study, our measured values for the Switzer Falls standard were $\delta^{34}S = 4.12 \pm 0.19$ ‰ (2σ) and $\Delta^{33}S = 0.00 \pm 0.16$ ‰ (2σ). The average sulfur content and standard deviation of the long-term laboratory blank was 0.18 ± 0.14 nmol (2σ), with a $\delta^{34}$S composition of 4.35 ± 7.98 ‰ (2σ) and these values were used to blank correct all ice core isotope measurements. Background samples taken before and after the S peak were used to calculate the concentration and isotopic composition of the volcanic sulfate end-member using:

$$\delta_{Volc} = \left(\delta_{measured} - f_{bkgd}\delta_{bkgd}\right) / f_{Volc} \quad (3)$$

where $\delta_{Volc}$ is the isotopic value of the volcanic sulfate, $\delta_{measured}$ is the measured isotopic value of the sample, $\delta_{bkgd}$ is the isotopic value of the background ice before or after the volcanic deposit and $f_{bkgd}$ and sulfate $f_{Volc}$ are the fractions of background and volcanic sulfate, respectively (Baroni et al., 2007; Gautier et al., 2019). Background corrected values are included for samples where more than 65 % of sulfate content comes from volcanic source. Samples with a lower fraction of volcanic sulfate (< 65 %) are unsuitable for this calculation due to large propagated uncertainties of the volcanic sulfate isotope compositions (Baroni et al., 2007; Gautier et al., 2018).

### 2.3. Tephra geochemistry

After centrifuging and removing the supernatant water for isotopic analysis, the remaining sample containing any potential tephra shards were combined with adjacent samples to reduce resolution and improve efficiency of tephra screening and analysis. This produced a total of 4 tephra samples across the 626 CE eruption peak, 6 samples for the 682 CE and 686 CE section, and 2 samples for the 698 CE eruption (Fig. 2; Table S1). Each combined tephra sample has a nominal time resolution of between 0.75 and 1.3 years.

Tephra samples were mounted in EpoThin2 epoxy resin following best practice procedures of (Innes et al., 2024; Iverson et al., 2017). Mounted samples were lightly polished using 6 μm, 3 μm, and 1 μm diamond suspension pastes for approximately 30 s to 1 min on each grade of polish. A final polish using 0.2 μm aluminium oxide polish was done for < 30 s.

Samples were screened for the presence of tephra by optical microscope and scanning electron microscope (SEM). Identified tephra shards were analysed for major and minor elements using electron probe microanalysis (EPMA) with a JEOL JXA-isp100 at the University of St Andrews electron microscopy facility. An accelerating voltage of 15 kV and beam of 5 μm and 5 nA was used for analysing glass shards in sample Tunu-167.25, corresponding to the particle peak at 686 CE where an abundance of tephra with a suitable size (≥5 μm) glass area were identified. All other tephra was analysed using a small beam size method with 3 μm and 1 nA beam conditions (Hayward, 2012; Innes et al., 2024). In a few cases where the tephra had a glass area < 3 μm, the beam was overlapped

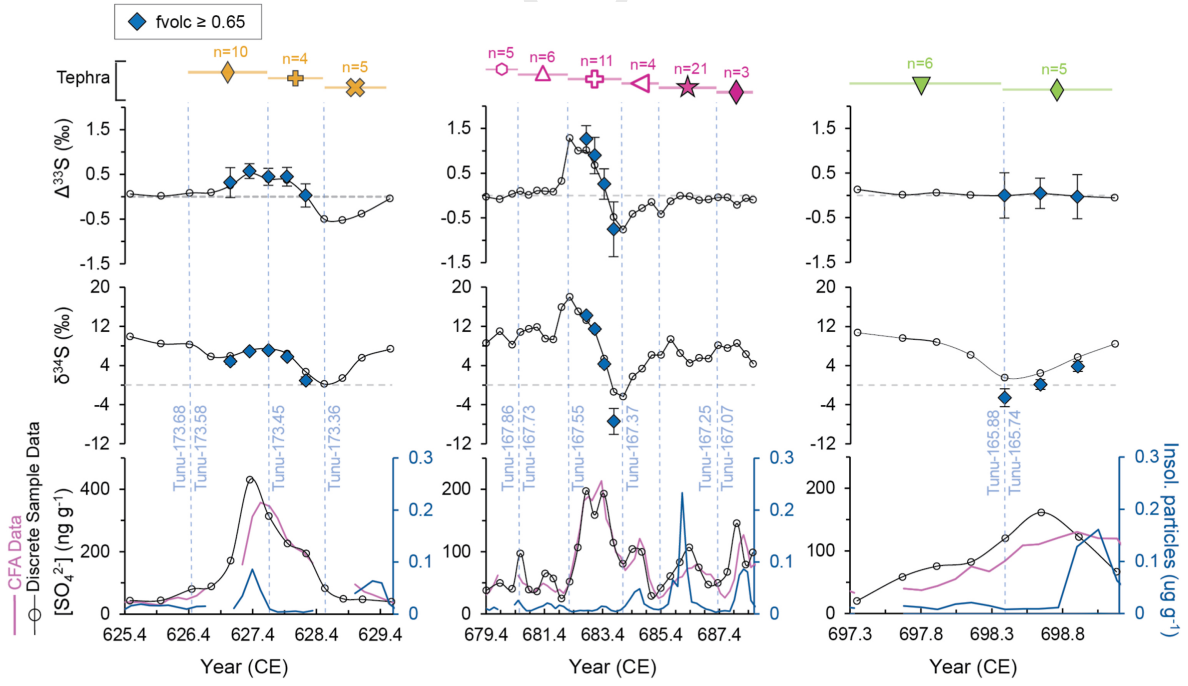


**Fig. 2.** Sulfate (black line, ng $g^{-1}$), 2.5-4.5 μm particle concentration (blue line, μg $g^{-1}$) (bottom row) and sulfur isotope analysis (middle and top rows) of sampled intervals of Greenland ice core Tunu2013, targeting volcanic events in 626, 682, 686 and 698 CE. Black circles in sulfate concentration and isotope plots represent measurements made on discrete samples. Horizontal dashed line in $\delta^{34}$S and $\Delta^{33}$S plots represent 0‰ line. For samples where the sulfate concentration was calculated to be >65% volcanic sulfate (fvolc ≥0.65), background corrected values are shown as blue diamonds. Error bars represent 2σ uncertainty for background corrected values. Vertical dashed blue lines through all plots show intervals combined for tephra analysis, preformed at lower time resolution than sulfur isotopes, and are labelled with sample identifiers referred to in text. Additional top line 'Tephra' shows the number of tephra shards identified and geochemically analysed in the interval. Samples plotted according to year of bottom depth, using Tunu2013 age model (Sigl et al., 2015).

on the epoxy resin (by up to 20 %). Although a decrease in precision is noted with the 3 μm beam overlap method, it has been shown to produce sufficiently accurate results to make robust geochemical ties between ice core cryptotephra and proximal deposits of identified eruptions (Innes et al., 2024). Some shards permitted multiple measurements with a 3 μm beam and in these cases, the average value of multiple analyses is plotted. Before, during and after sample analysis, the secondary standard glasses Lipari Obsidian ID3506, StHs6/80-G and ML3B-G (Jochum et al., 2006; Kuehn et al., 2011) were analysed to ensure standard calibration was appropriate and to monitor for instrumental drift. Low analytical totals (<95 %) from all methods of analysis, including the overlap method and with the beam fully positioned on the glass, were assessed on a case-by-case basis and only included in our dataset provided the normalised total was part of a geochemical population or grouped with other analysis with totals >95 %. Of 99 total analyses, 73 have analytical totals >95%, 15 have analytical totals of 90-95%, and 11 have analytical totals <90%. Of the shards with analytical totals <90%, 4 were discounted from our dataset for not grouping with a clear geochemical population (these analyses are still included in supplementary data). All major and minor oxide data from EPMA are normalised to 100% on an anhydrous basis in order to compare to source candidate geochemistry to assess for geochemical correlations. Similarity coefficients were calculated to provide statistical comparison between clear tephra groups identified and candidate volcanoes (Borchardt et al., 1972).

Eight tephra were analysed for trace element composition using laser ablation inductively coupled plasma mass spectrometry (LA-ICP-MS) using an Applied Spectra RESOlution SE Excimer laser ablation system coupled to an Agilent 8900 Triple Quadrupole ICP-MS system at the University of St Andrews STAiG laboratories. LA-ICP-MS was performed at 4 Hz with a fluence of 6 J/cm$^2$. Each analysis was completed using a 20 μm spot size, with acquisition time of 30 s. Calibration was performed using reference material NIST610 (Jochum et al., 2011). Secondary standards of rhyolitic tephras Old Crow and Lipari Obsidian ID3506 (Kuehn et al., 2011) were analysed at the start and throughout the analytical session and compared to available reference values (Kuehn et al., 2009; Maruyama et al., 2016). All data were reduced offline using Iolitev4.0 software (Paton et al., 2011), with internal standardisation using Al (previously measured using EPMA). Trace element concentrations used for correlations were within 10–20% of the reference values.

## 3. Results

### 3.1. Sulfur isotopes

Sulfate concentration and S isotopes of the Tunu2013 sub-samples are shown in Fig. 2 (626 CE isotopic data is previously published in Burke et al., 2023). Sulfur isotope analysis shows non-zero $\Delta^{33}S$ for the 626 CE and 682 CE eruptions (Fig. 2). The 626 CE eruption has a maximum background corrected $\Delta^{33}S$ of +0.57 ‰ (background corrected) followed by a negative $\Delta^{33}S$ minimum of −0.53 ‰ (not background corrected as fvolc <0.65). The first volcanic sulfate deposited from the 626 CE event does not carry a S-MIF signature (i.e. $\Delta^{33}S = 0$‰) and sulfur preserving the isotopic anomaly is deposited later in the peak. The 682 CE eruption deposit has a larger background corrected $\Delta^{33}S$ maximum of +1.28‰ followed by a negative minimum of −0.75‰ (Fig. 2). The sulfur carrying the S-MIF signature is deposited with the initial increase in sulfate concentration. The third targeted section containing the sulfate peak at 698 CE and the small increase in sulfate concentration coincident with the 686 CE particle peak are accompanied by decreases in $\delta^{34}S$ characteristic of volcanic sulfur deposits (Burke et al., 2019), but produce $\Delta^{33}S$ values within error of 0 ‰ (Fig. 2).

### 3.2. Tephra major element geochemistry

Tephra shards were identified in all samples apart from Tunu-173.68, immediately prior to the deposition of the 626 CE sulfate (Fig. 2). From the 626 CE sampled interval, 19 tephra shards were identified and analysed, from which two geochemical groups emerge (Fig. 3). A high FeO (>7.6 wt%), low $K_2O$ (<1.8 wt%) andesitic group (n = 7) of 10–15 μm size were found only in Tunu-173.58, coincident with the initial rise in sulfate concentration (Fig. 2). A second rhyolitic geochemical group from the 626 CE sampled interval cluster with high $K_2O$ (>4.0 wt%) and low (≤1 wt%) FeO and CaO content. This group, comprising of eight shards 10–40 μm in size, were found throughout the deposited sulfate peak in samples Tunu-173.58, Tunu-173.45 and Tunu-173.36. The andesitic tephra do not match the geochemistry of any known eruptions within dating uncertainty of the Tunu2013 626 – 627 CE ice core peak (Fig. 3; Table 1). The high-silica rhyolitic tephra shards show similarity to the large silicic eruption of Opala (Kamchatka) and North American tephra from the Southern Mono Craters. However, the high $K_2O$ (>4.0 wt%) rule out the 1.4 ka Opala eruption (Andrews et al., 2018; Plunkett et al., 2015; Ponomareva et al., 2017) as a candidate for this group, and low FeO and CaO (<1.0 wt%) rule out the most recent eruptions from the Southern Mono Craters (600-650 CE; Bursik et al., 2014; Jensen et al., 2021) as a source for all but one glass shard (~40 μm) identified in sample Tunu-173.58 (Fig. 3).

A total of 48 tephra shards were identified and successfully analysed from the sampled interval 680-690 CE targeting the 682 CE sulfate peak and 686 CE particle concentration peak. Sample Tunu-167.25, which includes the large peak in particle concentration at 686 CE (peak at 167.18 m; Fig. 1), was found to contain an abundance (n > 30) of 5–20 μm rhyolitic tephra, of which 21 analyses were made (Fig. 4). This population correlates across all measured oxides (similarity coefficient of 0.983; Table S3) with the Newberry Pumice tephra from the Big Obsidian period of Newberry volcano (Oregon, USA) (Jensen et al., 2021; Kuehn, 2002) extending the known distribution of this widespread North American cryptotephra to Greenland. Throughout the 680-690 CE sample set, 20 high-silica, low FeO and CaO rhyolitic tephras are identified and analysed (Fig. 4). Like the 626 CE rhyolitic group, these shards show geochemical coherence but no exact match to any silicic source candidates, except one larger (20 μm) shard in sample Tunu-167.07 which again matches the geochemistry of the Southern Mono Craters (Fig. 4). A small group (n = 3) of rhyolitic shards with higher $Al_2O_3$ (14.83 wt%) and FeO (1.57 wt%) in sample Tunu-167.55 are different in geochemistry from the other group of high-K rhyolite shards, but do not match geochemistry of any known eruptions occurring in this time interval. A further five shards from this sampled interval containing the 682 and 686 CE eruptions do not form any further geochemical populations.

For the 698 CE sampled interval, 11 tephra shards were identified and analysed. Eight of these found in both samples Tunu-165.88 and Tunu-165.74 are also geochemically similar to the highly silicic rhyolitic tephras in 626 and the 680–690 CE sampled interval. Geochemical variation of $K_2O$ (4.6–6.5 wt%) and $Na_2O$ (1.6–4.5 wt%) in the analyses of these shards make this population grouping less coherent than the other 626 CE and 680-690 CE tephras of similar rhyolitic composition (Fig. 6). The variation in alkali content may reflect alkali loss with small, thin shards present in the sample, or Na loss in glass impacted by weathering, as we do not see this degree of analytical variation in the secondary standards (see Supplementary Data). Again, despite similarities to the low-Fe and Ca rhyolitic 7th Century eruption candidates, no direct correlation is made to a known source, except for one shard which correlates with Southern Mono Crater geochemistry (40 μm in size, analysed twice). A further three tephra shards from these samples have lower $SiO_2$ than the high-K rhyolite shards, and do not form any groups or match any known eruption geochemistry (Fig. 5).

### 3.3. Tephra trace element geochemistry

Eight tephra shards were analysed for trace elements by LA-ICP-MS. Six shards were from the 626 CE sampled interval including three shards of the andesitic population (Tunu-173.58), one of the trachydacitic tephra (Tunu-173.58) and two rhyolitic tephra (one each from

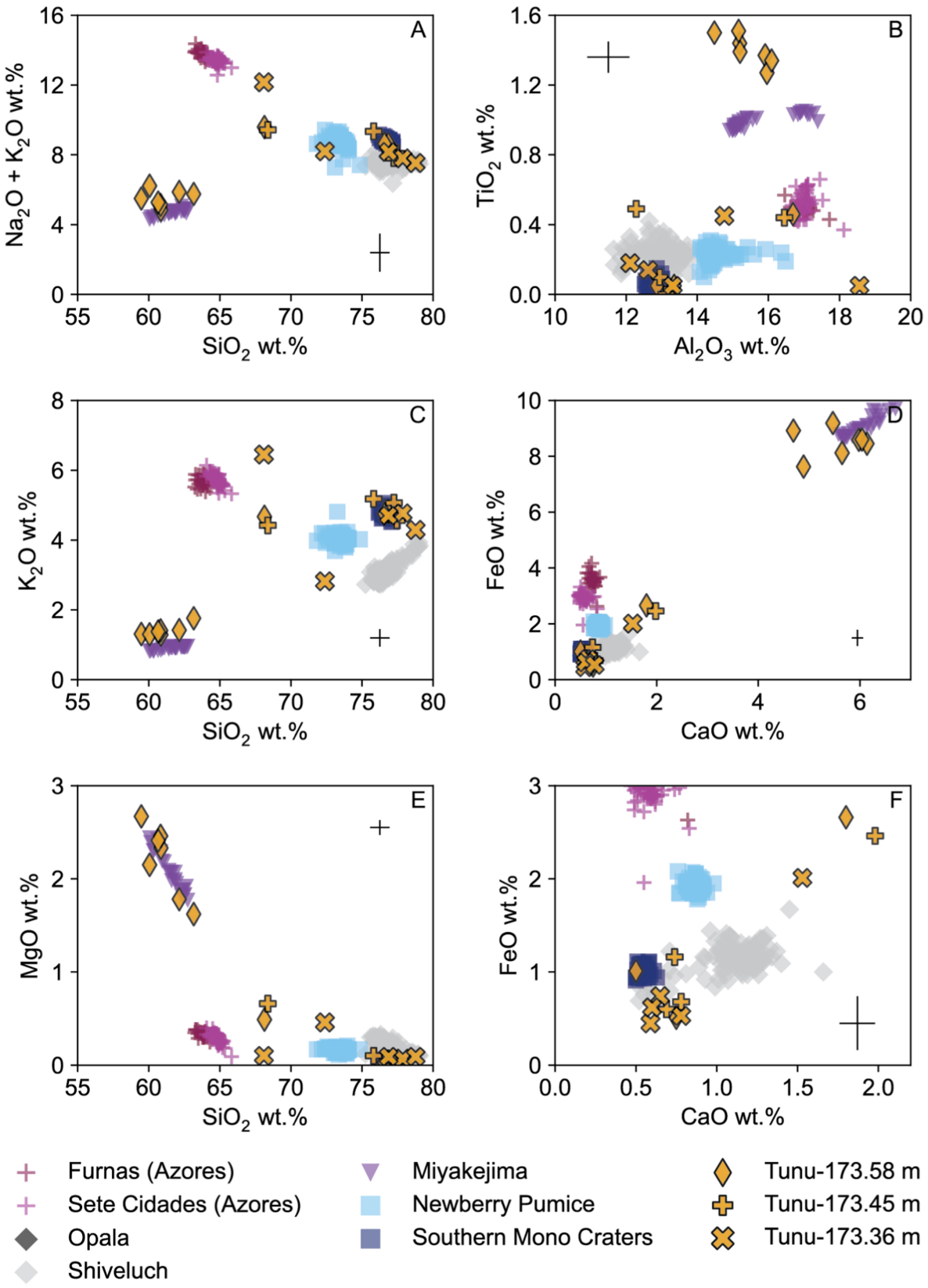


(*caption on next page*).

**Fig. 3.** Geochemistry of tephra from interval 173.68 m–173.19 m of Tunu2013 corresponding to the 626 CE extratropical stratospheric eruption deposit. Tephra compared to geochemistry of candidate extratropical eruptions as listed by the LaMEVE database (https://vogripa.org/) or hypothesised sources from literature discussed in the text. Newberry and Southern Mono Craters reference data from (Jensen et al., 2021), Kamchatkan candidates data (Opala and Shiveluch) from (Andrews et al., 2018; Plunkett et al., 2015; Ponomareva et al., 2015), Azores data (Furnas and Sete Cidades) from (Ellis et al., 2023; Wastegård et al., 2020), and Miyakejima (Japan) whole rock data from (Geshi et al., 2022). All data comes from analysis of glass tephra shards unless stated otherwise. Error bars represent 2σ uncertainty of glass standard Lipari ID3506 measured during analytical session.

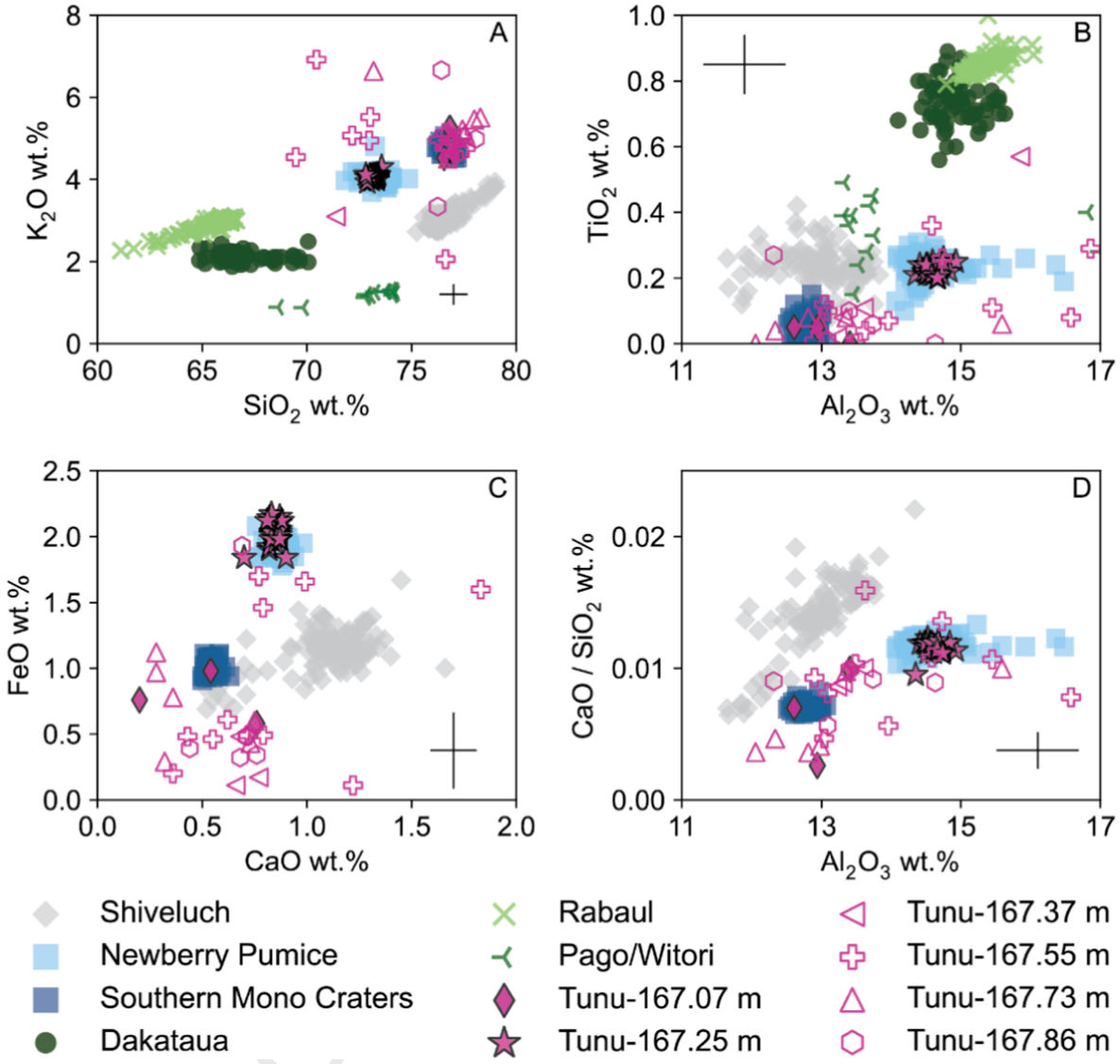


**Fig. 4.** Geochemistry of tephra from depth interval 167.85 m – 166.92 m corresponding to the large sulfate peak associated with the 682 CE tropical eruption, and the 686 CE particle peak (sample Tunu-167.25, magenta stars). Ice core tephra compared to geochemistry of tropical and extratropical eruptions that are considered most likely candidates as listed by the LaMEVE database (https://vogripa.org/), or hypothesised sources from literature. See Fig. 3 for geochemistry references for Newberry, Southern Mono Craters, and Shiveluch. New Britain Island eruption geochemistry for Dakataua, Rabaul and Witori from (Fabbro et al., 2020; Firth et al., 2024; Neall et al., 2021). Error bars represent 2σ uncertainty of glass standard Lipari ID3506 measured during analytical session.

Tunu-173.58 and Tunu-173.36). A further 2 rhyolitic shards from the 680-690 CE interval and 698 CE sample sets were analysed (one each from samples Tunu-167.07 and Tunu-165.88).

Based on their major element content, two rhyolitic shards from Tunu-167.07 and Tunu-165.88, along with one rhyolitic shards from sample Tunu-173.58 correlate with the Southern Mono Craters (Jensen et al., 2021). The trace element composition of these 3 shards are indistinguishable within analytical uncertainty and closely match trace element data from proximal Southern Mono Crater tephra and cryptotephras identified in North American bogs that are linked to this eruptive event (Fig. 7) (Jensen et al., 2021). In particular, the low Ba and Sr of the tephras is strongly characteristic of tephra originating from a rift setting, such as the Mono Craters. The second rhyolitic tephra analysed for trace elements from the 626 CE eruption set (Tunu-173.36) has higher Ba concentrations and does not show the same similarity to Southern Mono Craters trace elements (Fig. 7).

The 626 CE andesitic shards have consistent trace element concentrations except for Pb which shows greater variation across the 3 analyses. As secondary standard values are consistent and within 15% of other published concentrations (see Supplementary Data), the sample variation in Pb (11-61 ppm) is likely related to epoxy resin contamination from overlap of the 20 μm spot size when used on small (< 20 μm)

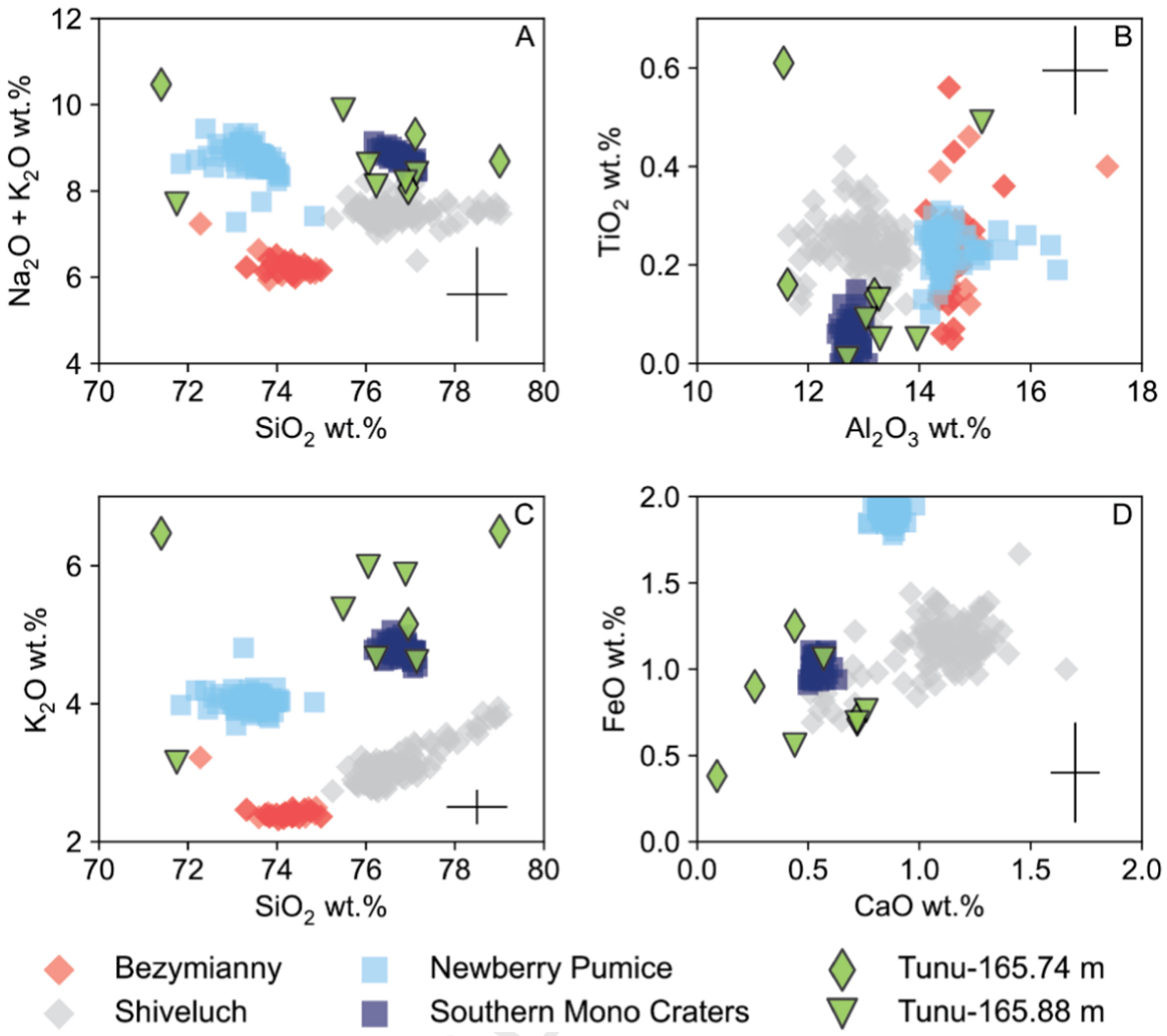


**Fig. 5.** Geochemistry of tephra from interval Tunu-165.88 m–165.62 m corresponding to the 698 CE high-latitude tropospheric eruption deposit. Tephra compared to geochemistry of candidate extratropical eruptions as listed by the LaMEVE database (https://vogripa.org/), or hypothesised sources from literature. See Fig. 3 for geochemistry references for Newberry, Southern Mono Craters, and Shiveluch. Bezymianny geochemistry of eruptions during last 2 ka from (Ponomareva et al., 2017). Error bars represent 2σ uncertainty of glass standard Lipari ID3506 measured during analytical session.

tephra. This does not appear to affect any other trace elements analysed.

## 4. Discussion

### 4.1. Newberry Pumice identification at 686 CE

The geochemistry of the abundant (≤20 μm) rhyolitic cryptotephra identified in sample Tunu-167.25 (particle peak at 167.13 m; Fig. 1) confidently correlates it to the Newberry Pumice tephra from Newberry Volcano, Oregon (Fig. 4). This VEI 4 eruption, which is radiocarbon dated to 635 ± 70 CE (Jensen et al., 2021), is part of Newberry's most recent 'Big Obsidian' eruptive period that comprised an initial explosive eruption followed by pyroclastic flows and lava flow activity (Gardner et al., 1998; Kuehn, 2002; Rust and Cashman, 2007). The widely dispersed ash fall from the Newberry Pumice eruption has previously been identified and geochemically characterised in bog and lake records in northeastern North America (Jensen et al., 2021; Pyne-O'Donnell et al., 2012). Our identification of this tephra in Greenland extends the known transportation distance to >5000 km and creates an important tie point between Greenland ice cores and the terrestrial North American records in which the Newberry Pumice tephra is found.

Our ice-core identification also allows us to improve on previous terrestrial radiocarbon age estimates (Jensen et al., 2021) and assign a more precise ice core age of 686 ± 2 CE to the eruption, as determined by the timing of Newberry Pumice tephra deposit in the Tunu2013 age model (Sigl et al., 2015). This precise ice core age for the Newberry Pumice contributes to reducing age model uncertainty for North American stratigraphic records during the first millennium CE, which have already been tied to Greenland ice cores at 852/853 ± 1 CE by the discovery of the White River Ash (east) marker (Coulter et al., 2012; Jensen et al., 2014; Mackay et al., 2022). Our new and precisely dated Newberry Pumice tie-point below the White River Ash (east) will further improve dating accuracy deeper in the stratigraphic record across the region.

Studies of the Newberry Pumice eruption show that the tephra fall deposit is characterised by elongated, easterly isopachs, leading to debate about whether the eruption was Plinian or sub-Plinian and whether isopleth mapping can be used to infer a reliable maximum column height for the eruption column (Gardner et al., 1998; Kuehn, 2002; Nathenson, 2017; Rust and Cashman, 2007). If taken as Plinian, the isopleths and tephra volume suggests maximum column heights of 21-25 km (Gardner et al., 1998; Kuehn, 2002; Nathenson, 2017), decreasing to 18 km as eruption intensity reduces midway through the eruption (Kuehn, 2002). Using particle size and thickness of the tephra deposits, Kuehn, (2002) inferred that prevailing wind speeds in excess of 50 m $s^{-1}$ (180 km $h^{-1}$) at the time of the eruption would have contributed to the distal ash trans-

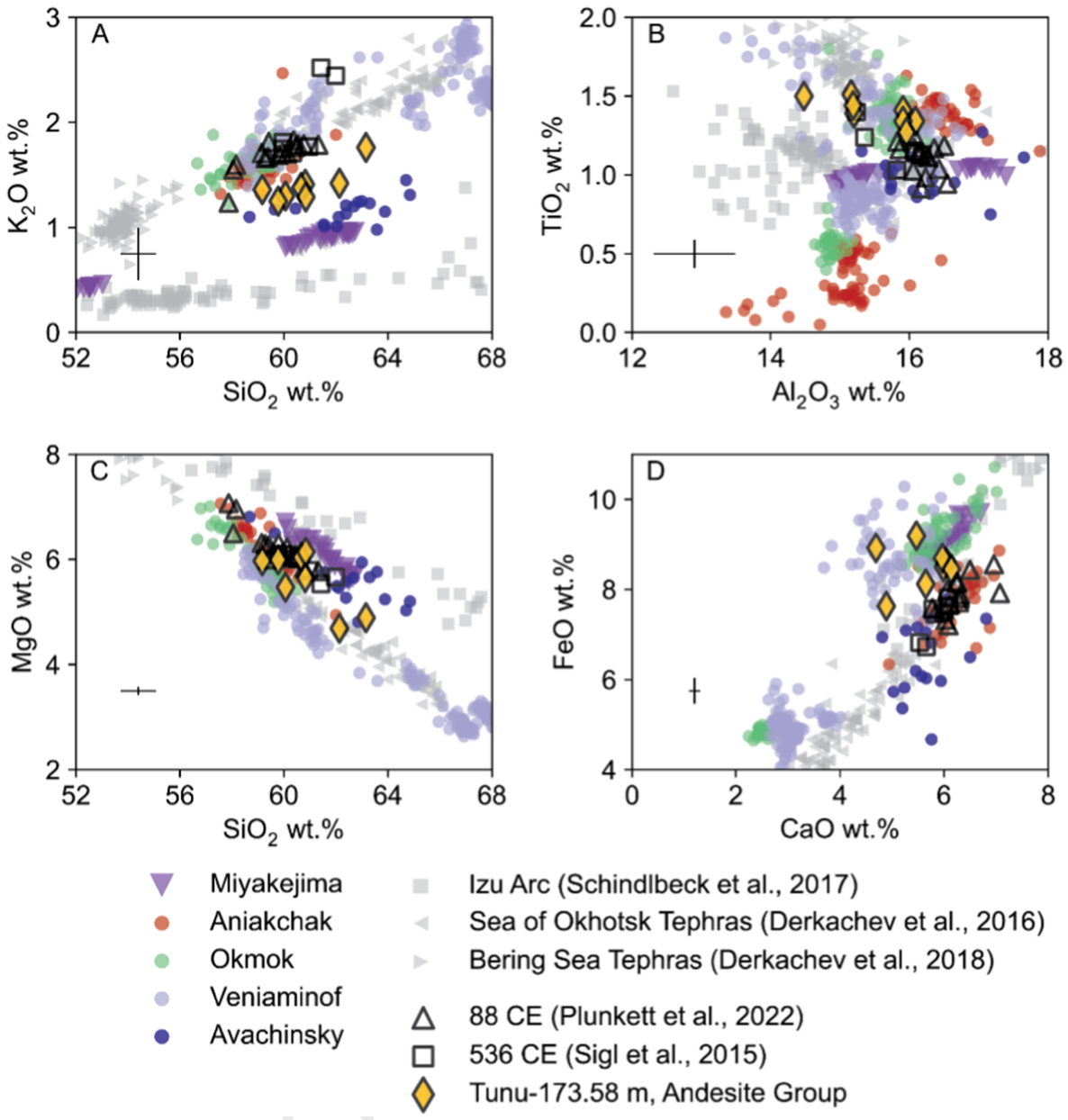


**Fig. 6.** Geochemistry of andesite tephra population (n = 6) identified at onset of 626 CE eruption sulfate peak, compared to geochemistry of Alaskan volcanoes Aniakchak, Okmok and Veniaminof and Kamchatkan volcano Avachinsky, known to produce andesitic products during explosive eruptions in the last 2000 years. Miyakekima whole rock geochemistry shown to be similar to 626 CE Andesite population in Fig. 3 is also plotted, alongside other Izu Arc and Quaternary tephras hypothesised to be from the North Pacific volcanic regions, identified in marine sediments. Also shown are ice core tephra identified alongside sulfate deposited from major climate-forcing eruptions in 536 CE and 88 CE (Plunkett et al., 2022; Sigl et al., 2015), hypothesised to originate from Eastern Aleutian Arc eruptions. Error bars represent 2σ uncertainty of glass standard Lipari ID3506 measured during analytical session. Geochemical data references: Aniakchak CFE II 3.6 ka eruption: (Davies et al., 2016); Okmok 43 BCE eruption: (Lubbers et al., 2023; McConnell et al., 2020); Veniaminof: (Lubbers et al., 2023); Avachinsky: (Krasheninnikov et al., 2020); Izu Arc Sediments: (Schindlbeck et al., 2017); Sea of Okhotsk tephras: (Derkachev et al., 2016); Bering Sea Tephras: (Derkachev et al., 2018).

port across the North American continent. Rust and Cashman, (2007) challenged these plume estimations because such high wind speeds would be more than two standard deviations faster than modern wind profiles for the region. Their interpretation is that the Newberry Pumice elongate isopachs represent a sub-Plinian eruption, which allowed for the plume to be more bent over by winds, and therefore column heights of 21-25 km are overestimated.

Sulfur isotope analysis can provide a further constraint on column height, because S-MIF should only be detectable for eruptions that inject significant quantities of sulfur in or above the stratospheric ozone layers. If the plume reached isopleth-derived altitudes of 21-25 km, S-MIF would be expected in our isotope analysis, as the ozone layer at extratropical latitudes (so including Newberry volcano at 43.7°N) is approximately 15-25 km (depending on season). In Tunu2013, the Newberry Pumice cryptotephra is accompanied by a small, but detectable increase in sulfate concentration (maximum sulfate peak of 107 ng $g^{-1}$) beginning in late-685 CE and peaking in 686 CE (Figs. 1 and 2). The S isotope data show no detectable S-MIF (i.e. $\Delta^{33}S = 0$ ‰), indicating the majority of the sulfur was unlikely to have been injected to altitudes 21-25 km (Fig. 2).

However, the volcanic sulfate peak associated with the Newberry Pumice tephra is only slightly elevated above background concentrations and thus it is possible our isotope measurements were not able to detect a small proportion of S-MIF carrying sulfate mixed with back-

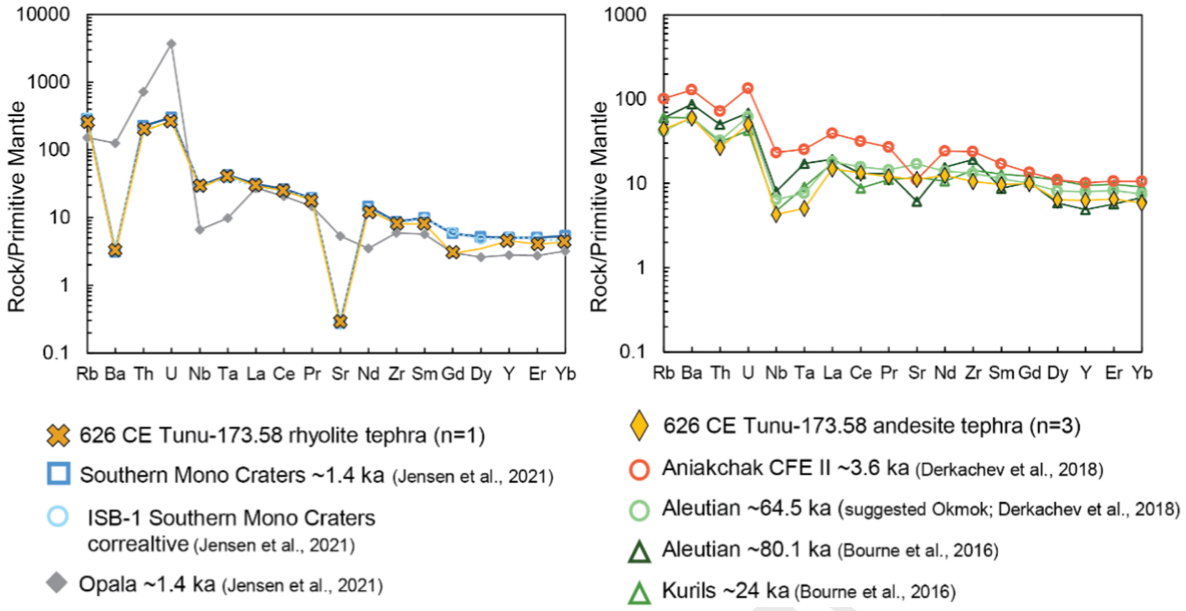


**Fig. 7.** Trace element geochemistry of tephra in sample Tunu-173.58 associated with the 626 CE extratropical eruption, after normalisation to Primitive Mantle (Sun and McDonough, 1989). Left panel shows single rhyolitic shard which matches Southern Mono Craters major and trace geochemistry (Jensen et al., 2021) and shows clear difference to Opala trace geochemistry. Right panel shows similarity of Tunu-173.58 Andesitic tephra (n = 3) to available trace element data of tephra identified in Bering Sea sediments (Derkachev et al., 2018) and Greenland ice cores (Bourne et al., 2016) linked to Quaternary eruptions of Pacific Arc volcanoes.

ground and tropospheric aerosol. To test this, we can use isotope mass balance to calculate the maximum proportion of stratospheric sulfate (carrying a S-MIF signature) that could be present in the Newberry Pumice ice core deposit that would still result in a measured $\Delta^{33}S$ of 0 ‰. As our 2σ uncertainty for $\Delta^{33}S$ is ±0.16 ‰, we consider this to the threshold for a identifying an S-MIF signal. By subtracting the estimated ice core background sulfate concentration (39 ng $g^{-1}$) from the maximum peak of sulfate concentration associated with the Newberry Pumice in Tunu2013 (106 ng $g^{-1}$), we estimate that the total sulfate in the ice ($f_{total}$) is comprised of 63% volcanic sulfate ($f_{volc}$) from the Newberry eruption and 37% of background sulfate ($f_{bkgd}$). The volcanic sulfate deposited (63% of $f_{total}$) is itself made up of the sum of stratospherically ($f_{strat}$) and tropospherically ($f_{trop}$) transported sulfate, which could vary depending on plume height, transportation pathways, and proximity of the eruption to the ice core site. Our isotope analysis of Tunu2013 background ice core samples assumed to be unaffected by volcanic events carry a $\delta^{34}S$ of 9.48 ± 1.2 ‰ (n = 6), and a $\Delta^{33}S$ of 0 ‰, and tropospheric volcanic sulfate not exposed to UV photochemistry also carries a mass dependently fractionated $\Delta^{33}S$ signature of 0 ‰, and estimated $\delta^{34}S$ of 4.1 ± 0.5 ‰ (Jongebloed et al., 2023). Based on sulfur isotope studies of large, tropical eruptions of the Common Era, volcanic sulfate transported purely through the stratosphere and mass independently fractionated by UV photochemistry typically carries a maximum $\Delta^{33}S$ of 1–2 ‰ (Burke et al., 2019; Gautier et al., 2018). We then use the following isotope mass balance equation to calculate the maximum fraction of stratospheric sulfate present:

$$\Delta^{33}S_{measured} = f_{volc}(f_{strat}\,\Delta^{33}S_{strat} + f_{trop}\,\Delta^{33}S_{trop}) + f_{bkgd}\,\Delta^{33}S_{bkgd} \quad (4)$$

rearranged to solve for $f_{strat}$, assuming that $f_{trop} = 1 - f_{strat}$ :

$$f_{strat} = \frac{\Delta^{33}S_{measured} - f_{volc}\Delta^{33}S_{trop} - f_{bkgd}\,\Delta^{33}S_{bkgd}}{f_{volc}(\Delta^{33}S_{strat} - \Delta^{33}S_{trop})} \quad (5)$$

where $\Delta^{33}S_{measured}$ is the ice core deposit $\Delta^{33}S$ from sulfur isotope analysis (assumed to be 0.16 ‰ due to our 2σ uncertainty on $\Delta^{33}S$), $\Delta^{33}S_{strat}$ is the assumed $\Delta^{33}S$ range (1–2‰) of stratospherically transported sulfate, $\Delta^{33}S_{trop}$ is the $\Delta^{33}S$ of tropospherically transported volcanic sulfate carrying no S-MIF (0 ‰), and $\Delta^{33}S_{bkgd}$ is the $\Delta^{33}S$ of background ice core sulfate, also carrying a mass dependent $\Delta^{33}S$ of 0 ‰. We calculate the maximum fraction of stratospheric sulfate present in the Newberry Pumice Tunu2013 ice core deposit to be 12% and 25%, if $\Delta^{33}S_{strat}$ is 2.0 ‰ and 1.0 ‰ respectively. This suggests that a portion of the Newberry sulfur gas plume could have reached altitudes in or above the ozone layer as suggested by isopach approximations, but that the majority that was deposited in Greenland (75-88 %) was transported via the troposphere.

An additional caveat is that plume heights derived from isopleths are usually higher than the $SO_2$ injection height (based on study of satellite-era eruptions (Aubry et al., 2023)). This satellite era compilation shows the average ratio of isopleth height to tephra column top height is 1.45, and the average ratio of $SO_2$ injection height to column top height is 0.97. Assuming the previously calculated Plinian 21-25 km isopleth heights are accurate, this would suggest $SO_2$ injections were likely around 14-17 km (using a scaling factor of 1.49; Aubry et al., 2023; Hutchison et al., 2025), in agreement with our estimated sulfur gas plume altitude from sulfur isotope analysis that suggest the majority (minimum 75 %) of the sulfur was transported below the stratospheric ozone layer (the bottom of which is ~16 km at the latitude of Newberry volcano).

As well as constraining plume height, the identification of Newberry Pumice in Greenland has important implications for understanding the risk of moderate (VEI 4) eruptions in terms of ash dispersal. The detection of tens of tephra shards in Greenland ice suggests that given favourable wind conditions, there is potential for ash up to 20 μm in size, to reach several thousand kilometres across North America, Greenland and the wider North Atlantic region (discussed further in Section 4.5).

### 4.2. 626 CE Northern Hemisphere eruption

Sulfur isotopes from the 626 CE sulfate peak in the Tunu2013 ice core (Fig. 2) show that the initial volcanic sulfate does not carry any S-MIF signal (i.e. $\Delta^{33}S$ = 0 ‰). It is then followed by a muted positive peak of $\Delta^{33}S$ = +0.57 ‰ (corrected for background sulfur) when the volcanic sulfate transported via the stratosphere is deposited (Burke et al., 2023). Burke et al. (2023) assigned this to an extratropical source, as the initial mass dependent sulfur signature from the input of tropospheric sulfate requires a source proximal to the ice sheet (Burke et al., 2019). The pro-

portion of sulfate deposited on the ice sheet that was transported via the stratosphere has been previously calculated by (Burke et al., 2023) using isotopic mass balance equations as 75 ± 9 %.

Tephra identified with the 626 CE ice core sulfate do not correlate with a known Northern Hemisphere eruption. The only exception is the single rhyolitic shard (in sample Tunu-173.58 m); that matches the Southern Mono Craters eruption geochemistry across major and trace elements (Fig. 3; Fig. 7). However, no other tephra show a close match to this eruption, with the subtle differences in major and trace element data suggesting that the high-K rhyolitic tephras associated with the 626 CE eruption could be from multiple sources, discussed further in Section 4.5.

The andesitic tephra population in sample Tunu-173.58 (n = 6) was deposited coincidently with the initial increase in tropospheric sulfate at 626 CE. This synchronous timing of the tephra and sulfate deposition is characteristic of extratropical eruptions (Abbott and Davies, 2012; Hutchison et al., 2025; Plunkett et al., 2023), suggesting that they originate from the same source.

The tephra composition shows similarity to geochemistry of the VEI 4 Suoana-Kazahava eruption of Japanese Izu arc volcano Miyakejima (radiocarbon dated to 644-680 CE) (Geshi et al., 2022). However, higher $TiO_2$ of the Tunu2013 tephra rules out a confident link when directly comparing available whole rock data of aphyric ejecta samples (Geshi et al., 2022) with ice core tephra glass shards (Fig. 3). There are also differences in major oxides for other much older (0.3 – 1 Ma) basaltic-andesitic Izu Arc eruptions (Schindlbeck et al., 2017) and tephras from the Sea of Okhotsk and Bering Sea sediments (Derkachev et al., 2016, 2018) (grey symbols in Fig. 6). Future direct comparison of glass geochemistry would rule out any potential uncertainty associated with crystallisation of whole rock samples that may cause differences in major elements, including $TiO_2$, and better confirm or discount a link between Tunu2013 626 CE tephra and Miyakejima and other Holocene Izu Arc eruptions.

There are no other known ≥ VEI 4 andesitic eruption candidates from extratropical latitude Northern Hemisphere sources reported within uncertainty of the 626 CE eruption (Table 1). Trace element analysis provides further information about tectonic setting, with marked depletion in high field strength elements Th, Nb and Ta (Fig. 7) characteristic of subduction settings (Bourne et al., 2016; Tomlinson et al., 2015). This rules out Icelandic volcanism as a source of the ash and points instead towards North Pacific volcanic arcs as the closest systems most likely to deposit tephra in Greenland. As well as Miyakejima and Izu arc eruptions, the Tunu2013 626 CE tephra major and minor element geochemistry bears a close resemblance to andesitic eruptions of Eastern Aleutian Arc (EAA) volcanoes, including Aniakchak, Okmok and Veniaminof, known to produce explosive, climatically significant eruptions during the last few thousand years with tephra transport from the region to the Greenland ice sheet (Fig. 6) (McConnell et al., 2020, 2025; Pearson et al., 2022). The TephraKAM geochemical database for the Kamchatka volcanic arc (Portnyagin et al., 2020) also lists high-FeO and CaO andesitic eruptions of Kamchatkan volcano Avachinski (Krasheninnikov et al., 2020) in the first millennia CE, which have geochemistry characteristic of, but not identical to the tephra identified in Tunu-173.58 m (Fig. 6). Calculated similarity coefficients show the closest geochemical match is to the low-Si component of tephra from the Okmok 43 BCE eruption (SC = 0.92; Table S3) (McConnell et al., 2020), strengthening the hypothesised link to EAA systems. The trace element data from analysis of three andesitic shards shows a similar trend to proposed Kuril and Aleutian tephras (Fig. 7) identified in marine sediments (Derkachev et al., 2018) and Greenland ice cores (Bourne et al., 2016). While this data is from late-Quaternary deposits which are much older than the eruptions investigated in this study, it provides a useful comparison to demonstrate the consistency of trace element pattern between the ice core tephra identified at 626 CE and suggested Pacific arc source regions.

Comparison of ice core tephra trace element data to available trace element data of North Pacific eruptions identified in marine sediments) and an ice core tephra suggested to be of Kuril origin shows the trace elements also show a similar trend to these North Pacific arc systems (Fig. 7).

The 626 CE andesitic tephra population we identify is very similar in composition to the tephra population associated with in the 88 CE volcanic sulfate peak in the NEEM-2011-S1 ice core (Plunkett et al., 2022) and one of the tephra populations associated with the climatically important 536 CE extratropical eruption (Burke et al., 2023; Sigl et al., 2015) (Fig. 6). These previous studies also suggest EAA volcanoes as probable sources for the 88 and 536 CE tephra found in Greenland ice. These attributions, as well as our conclusions for the andesitic 626 CE tephra, suggest EAA or Kamchatkan sources for both the first and last major eruptions of the Late Antique Little Ice Age (LALIA) sustained cold period from ~536 to 640 CE, with notable societal impacts across the Northern Hemisphere (Büntgen et al., 2016; Fei et al., 2007). While there have been Holocene tephrochronological studies in Alaska and Kamchatka (Bolton et al., 2020; Braitseva et al., 1997; Davies et al., 2016; Fortin et al., 2019; Plunkett et al., 2015; Ponomareva et al., 2017; Praet et al., 2022; Riehle, 1985) the absence of clear links to known and dated eruptions suggests major gaps remain in our understanding of eruptive histories from these remote regions.

The presence of other tephra populations including the rhyolitic tephra deposited throughout the 626 CE samples and two trachydacite shards of unknown source in samples Tunu-173.58 and Tunu-173.45 means we cannot rule out multiple, climate impacting eruptions at this time. However, the occurrence of a geochemically consistent population of andesitic tephra in a single sampled section coincident with the initial tropospheric sulfate, points towards an andesitic, North Pacific volcanic arc eruption as the most likely source of the extratropical 626 CE eruption recorded in Greenland ice.

### 4.3. 682 CE tropical eruption

Sulfur isotope analysis identifies a large stratospheric aerosol deposit from an eruption in 682 CE, shown by the presence of S-MIF (Fig. 2). A clear time evolution of the isotopic anomaly is observed with an initial positive peak in $\Delta^{33}S$ followed by negative $\Delta^{33}S$ deposited over a timescale of 2–3 years. This signature is characteristic of a large tropical eruption, as all volcanic sulfur deposited carries the S-MIF signature and $\Delta^{33}S$ increases with the initial growth of the sulfate concentration peak (Burke et al., 2019; Gautier et al., 2018). Previous sulfur isotope analysis (performed at lower time resolution) of the corresponding volcanic sulfate peak at 682 CE at Dome C, Antarctica, by Gautier et al. (2019) records a $\Delta^{33}S$ anomaly of $-0.63 \pm 0.06$ ‰ (1σ). This bipolar S-MIF signal is consistent with the attribution of the 682 CE event to a large tropical eruption (Sigl et al., 2015).

Compared to some of the largest eruptions and $\Delta^{33}S$ measurements of the Common Era (Samalas in 1257 $\Delta^{33}S = +1.7$–$2.2$ ‰, and Tambora in 1815 $\Delta^{33}S = +1.7$‰; Burke et al., 2019; Gautier et al., 2019, 2018), the maximum background corrected $\Delta^{33}S$ of +1.27 ‰ for the 682 CE eruption is smaller, reflecting either a lower altitude (Crick et al., 2021) or potentially a less optically thick sulfate cloud than the largest eruptions of the Common Era, if the mechanism for S-MIF is photolysis self-shielding (Endo et al., 2024). However, this non-zero $\Delta^{33}S$ signal provides evidence that the tropical 682 CE eruption had a sulfur plume that reached the ozone layer.

Candidate tropical eruptions for the 682 CE ice core volcanic deposit include the large (VEI 5-6) eruptions of Rabaul, Witori, and Dakataua from New Britain Island, Papua New Guinea (Gao et al., 2016; McKee et al., 2011, 2015; Sigl et al., 2015). Smaller (VEI 4) Central American eruptions of Arenal in ~650 CE (Bolge et al., 2006), Cotopaxi in ~740 CE (Hall and Mothes, 2008), and El Chichón ~700 CE (Espíndola et al., 2000) also have been suggested as a candidates for sulfate peaks in ice cores between 670 and 730 CE (Gao et al., 2016), but simulations of ash dispersion and deposition (Plunkett et al., 2022) show it is unlikely that ash from VEI 4 tropical eruptions could reach Greenland. To date, only

ash from more powerful ≥ VEI 6 Common Era eruptions at tropical latitudes has been identified in Greenland ice (e.g. (Hutchison et al., 2024; Smith et al., 2020) and, therefore, these smaller magnitude eruptions can tentatively be ruled out as sources for the ice core deposits. As we do not identify any dacitic-andesitic shards in our Tunu2013 samples associated with the 682 CE eruption, no geochemical correlation has yet been confirmed between the widely hypothesised candidate VEI 5-6 New Britain Island eruptions and the 682 CE sulfate in Greenland ice (Fig. 4). Future research targeting tephra identification for the Antarctic counterpart of the 682 CE peak (Fig. 1) also known to carry an S-MIF anomaly (Gautier et al., 2019) may provide more robust conclusions about the eruption source.

Although we do not identify the specific volcanic source, the S-MIF isotopic signature confirms that all the volcanic sulfur deposited in Greenland from the 682 CE eruption has been transported via the stratosphere. Using the quantity of sulfur deposited in ice cores, the volcanic stratospheric sulfur injection (VSSI) of the 682 CE eruption has been estimated at 27.2 Tg S (Toohey and Sigl, 2017), approximately the same as the Tambora 1815 CE eruption (28.1 Tg S) and ~45% of the 1257 CE Samalas eruption which has the highest VSSI of the Common Era (59.4 Tg S; Toohey and Sigl, 2017). This ranks the 682 CE eruption as the 7th largest of the last 2500 years in terms of VSSI. resulting in a climate cooling of ~1 °C based on temperature reconstructions across Europe and the Arctic (PAGES 2k Consortium, 2013; Sigl et al., 2015). A more prolonged period of Northern Hemisphere cooling is initiated by this eruption (Gao et al., 2016), with southern Colorado Plateau bristlecone pine tree ring-based temperature records showing a cold temperature anomaly initiated in 683 CE, and sustained until the end of the 7th Century (Salzer and Kipfmueller, 2005). This particular episode of volcanic induced cooling has been linked with severe societal disruption, especially in China, Japan and Europe (Büntgen et al., 2025; Di Cosmo et al., 2017; Gao et al., 2016).

### 4.4. 698 CE Northen Hemisphere eruption

Sulfur isotope data shows that all the sulfate deposited from the 698 CE event is tropospheric and from an extratropical eruption proximal to Greenland. This finding disproves previous assumptions that the 698 CE eruption was tropical (Sigl et al., 2015) and instead suggests that the contemporaneous sulfate deposit in Antarctica is from a high latitude eruption in the Southern Hemisphere. (Fig. 1). Future investigation of the Antarctic counterpart peak at 698 CE may provide further insights to confirm the volcanic source origins of the sulfate.

Although several rhyolitic tephra shards are identified, they do not conform to a consistent geochemical grouping which suggests there may be contributions from multiple volcanic sources. Aside from the single, largest (~30 μm) shard from 698 CE which is geochemically indistinguishable from proximal tephra of the Southern Mono Craters (Jensen et al., 2021) (Fig. 5), the tephra do not match any known, Northern Hemisphere extratropical candidates. In distal terrestrial samples, a Southern Mono Craters correlative (ISB-1/BB-2/SB-5 in Jensen et al., 2021) is deposited prior to the Newberry Pumice tephra (which we show here to be in 686 CE). This stratigraphic relationship suggests that this shard, and the one at ~687-688 CE in sample Tunu-167.07, are not directly linked to the Southern Mono Craters correlative in Jensen et al. (2021) as they are deposited in the ice core after the Newberry eruption. Proximal deposits from the Southern Mono Craters show that after an initial release, the sequence involved multiple smaller, short lived eruptive pulses and a complex progression switching among numerous vents (Bursik et al., 2014), which may explain the multiple occurrences of Mono Craters correlating tephra in the Tunu2013 ice core over these sampled time intervals. It is possible that Tunu2013 insoluble particle peaks in 650 and 666 CE may represent the initial Plinian Southern Mono Craters eruption (Fig. 1) and future investigation of these deposits may resolve current uncertainties about the Southern Mono Craters eruption timeline. The challenges of attributing these single shards are discussed more in the following Section (4.5)

### 4.5. Wider implications, opportunities and challenges

Our work demonstrates how combining sulfur isotope and tephra geochemical analysis is a powerful approach for better constraining source parameters of volcanic eruptions recorded in ice cores, especially when there is little or no historically documented evidence. The most notable success of combining these for eruptions during the 7th Century of the Common Era is identification of the Newberry Pumice using tephra geochemistry (Section 4.1). While this tephra identification alone provides a high-precision age for the Newberry Pumice eruption and an important stratigraphic tie between terrestrial and ice records, the sulfur isotope analysis offers additional constraints on sulfur injection height, which in this case was largely confined to the troposphere (Section 4.1). The success of these methods is further demonstrated when applied to eruptions in 626, 682 and 698 CE, considered to be related to periods of cooling identified in climate proxy records for the Northern Hemisphere. Although we do not pinpoint the exact sources for these eruptions, sulfur isotope analysis informs source latitude constraints, and tephra geochemistry allows us to rule out known major eruptions that are radiocarbon dated to windows spanning the 7th Century as potential candidates (e.g. extratropical candidates Opala and Shiveluch for the 626 CE eruption; Section 4.2). In particular, the sulfur isotope signature of the 698 CE deposit demonstrates that coincident sulfate peaks in Greenland and Antarctica do not always indicate a tropical eruption sources (Sigl et al., 2015). Contributions such as these are of key importance to reconstructing Earth's volcanic record prior to the satellite era and providing the most accurate forcing records for climate models. In practical terms, our combined tephra and sulfur isotope approach not only provides multiple constraints on past eruptions (e.g. plume height, latitude, tectonic setting, VSSI), but they make the most of precious ice core resources.

This work also highlights the challenges of relating ultra-distal ice core cryptotephras to specific sources. Using a higher time-resolution sampling method and small EPMA beam sizes allows identification and analysis of very small (< 10 μm) cryptotephra. In cases such as the 686 CE Newberry Pumice tephra, or the 626 CE andesitic tephra, there are clear populations with overlapping chemistries that can be used to link the ice core sulfate to a known source or tectonic setting. However, as discussed in Sections 4.3 and 4.4, the high-K rhyolitic tephra analysed from the 680-690 CE interval and 698 CE eruption sample sets are more dispersed and do not form clear geochemical groups. The persistence and geochemical spread of these tephra create a challenge for identifying if this rhyolitic tephra is primary airfall tephra from an eruption, multiple eruptions or pulses of the same system, as has been suggested for the formation of the Mono Craters (Bursik et al., 2014; Putnam, 1938; Sieh and Bursik, 1986), or a secondary remobilisation of volcanic dust that is transported to Greenland. Although no obvious morphological signs of weathering were observed for tephra shards analysed, major element analysis gives some indication to aid distinction between primary and secondary deposits in the Tunu2013 samples, with lower $Na_2O$ totals (< 3 wt% in rhyolitic glasses) suggestive of weathering for shards with rhyolitic geochemistry (see supplementary data). This broader issue is one discussed in previous studies (Plunkett et al., 2023) for the identification of recurring, low abundance tephras in ice core samples, usually high in silica and low (≤1 wt%) in FeO and CaO. As interest increases in cryptotephra samples where only a few shards are available for analysis, consideration must be given to this complex issue in order to differentiate what may be background contributions of weathered and remobilised shards to the ice core record and genuine primary ash deposition.

As our ability to detect and geochemically characterise extremely fine, sparse tephra shards in distal records (such as polar ice cores) improves, we may be able to detect eruptions that have more episodic eruption style, such as the style of activity described at the Southern Mono

Craters (Bursik et al., 2014). For deposits of more abundant, geochemically indistinguishable tephra deposits, challenges remain for correlation to known volcanic systems. No known eruptions are dated to within uncertainty of the 626 CE Tunu2013 deposit which match the andesitic geochemistry of the tephra group identified. While we demonstrate that this group show affinity to some Aleutian, Kamchatkan, and Japanese arc system volcanoes, the sparse historical records and limited and/or complex proximal stratigraphic sequences in these remote regions of active volcanism makes the correlation of ice core tephra with sources problematic, with similar issues recognised in studies of other Northern Hemisphere eruptions associated with climate cooling (Hutchison et al., 2025; Plunkett et al., 2022; Sigl et al., 2015).

Despite these challenges, the outcomes of this study contribute to fundamental understanding of the risks and hazards posed by stratospherically transported sulfate and far travelled fine ash associated with Northern Hemisphere volcanism. The extratropical attribution of the 626 CE eruption supports recent studies showing that there is increased summer temperature climate sensitivity to stratospheric sulfur injections from Northern Hemisphere extratropical eruptions (Burke et al., 2023; Toohey et al., 2019). Our first identification of the Newberry Pumice tephra in Greenland highlights the potential hazards of VEI 4 eruptions to the North Atlantic region. The abundance of very fine grained ($\leq$20 μm) tephra shards reaching $>$5000 km from Newberry volcano itself suggest material from the plume was carried even further than Greenland. If a similar event was to occur today, with favourable, strong wind conditions such as those suggested at the time of the 686 CE Newberry eruption (Kuehn, 2002), the distribution of fine ash material would cause significant disruption across North America and transatlantic airspace. Previous tephra from the North Pacific region identified in Greenland have originated from eruptions several magnitudes greater than the Newberry Pumice (e.g. VEI 7 Mazama Ash (Davies et al., 2024); VEI 6 WRAe (Coulter et al., 2012; Jensen et al., 2014); VEI 6 Aniakchak CFEII (Pearson et al., 2022)). Our identification of the Newberry Pumice eruption confirms that given favourable transport conditions, smaller and more common (i.e. VEI 4) eruptions from the western North America and northern Pacific systems have the potential to distribute fine ash several thousand kilometres from the eruption site, posing a greater risk than previously thought to the airspace of more distal regions (Bourne et al., 2016; Jensen et al., 2014, 2021; Wang et al., 2025; Watson et al., 2017).

## 5. Conclusion

Using sulfur isotope and geochemical analysis of tephra shards identified in the Tunu2013 ice core from Greenland, we improve understanding of source parameters for four major volcanic eruptions during the 7th Century of the Common Era. We correlate a peak in particle concentration at 686 ± 2 CE with the Newberry Pumice tephra, extending the known ash distribution of this eruption to Greenland, and infer that the majority of the sulfur plume was transported below the stratosphere, based on sulfur isotope analysis. This finding demonstrates the risk that VEI 4 eruptions can pose to the North Atlantic region, with fine ($<$20 μm) tephra transport over 5000 km from the source. We use sulfur isotopes to confirm previous assumptions of extratropical, and tropical source latitude for eruptions in 626 and 682 CE, respectively. We also revise the previous assumption of a tropical latitude eruption responsible for the 698 CE Tunu2013 sulfate deposit, to an extratropical Northern Hemisphere source due to a non-S-MIF isotopic signature.

We identify tephra shards throughout the sampled intervals for each of these eruptions, which we compared to the geochemistry of known $\geq$ VEI 4 eruptions dated within uncertainty of the ice core peaks. No direct correlations were made between these candidates and the ice core tephra groups identified for the extra tropical 626 CE, tropical 682 CE, or extratropical 698 CE eruptions. However, geochemistry of tephra deposited with the sulfate peaks of 626 and 698 CE prove useful for ruling out major rhyolitic eruptions of Kamchatkan volcanoes Opala and Shiveluch, and Azores eruptions of Furnas and Sete Cidades as candidate sources for the Northern Hemisphere eruptions. An andesitic population of 6 tephra shards deposited with the 626 CE eruption show close similarity to eruptions of Aleutian, Kamchatkan, and other Pacific arc volcanoes, leading us to conclude that the most likely source of the 626 CE ice core deposit is a currently unrecorded eruption from these regions. Sulfur isotopes and tephra geochemical analysis of other sulfate and insoluble particle peaks recorded in Greenland ice cores during the 7th Century (e.g., 650, 666, 689 and 694 CE; Fig. 1) may link ice cores with other hypothesised sources in this study and provide a more complete assessment of volcanism from this time period. These insights contribute to ongoing efforts to better interpret the ice core volcanism record, providing more accurate eruption source parameters for eruptions linked with major climate responses of the Common Era.

## Author contribution

AB: Conceptualization, Funding acquisition, Methodology, Project administration, Resources, Supervision; HI: Conceptualization, Formal analysis, Funding acquisition, Investigation, Methodology, Project administration, Visualization, Writing – original draft; JRM: Formal analysis, Methodology, Resources; MS: Formal analysis; NJC: Formal analysis; JTS: Formal analysis; WH: Methodology, Project administration.

Writing – review and editing: All authors.

## Declaration of competing interest

The authors declare that they have no known competing financial interests or personal relationships that could have appeared to influence the work reported in this paper.

## Acknowledgements

This work was supported by a NERC IAPETUS2 DTP studentship [NE/S007431/1] awarded to H.M.I. W.H and H.M.I are funded by a UKRI Future Leaders Fellowship [MR/S033505/1] awarded to W.H. A.B. is funded by a Horizon Europe Guarantee Grant [EP/Z000645/1] and a NERC Grant [NE/Y001028/1]. The Electron Microscopy Facility at the University of St Andrews is supported by EPSRC grants EP/L017008/1, EP/R023751/1 and EP/T019298/1. Our thanks to Gill Plunkett who provided comments on an earlier version of this manuscript.

## Appendix A. Supplementary data

Supplementary data to this article can be found online at https://doi.org/10.1016/j.quascirev.2026.110036.

## Data availability

All data and/or code is contained within the submission.https://doi.org/10.17630/d219f650-9edf-4a8f-babe-10f5f8747334

## References

Abbott, P.M., McConnell, J.R., Chellman, N.J., Kipfstuhl, S., Horhold, M., Freitag, J., Cook, E., Hutchison, W., Sigl, M., 2024. Mid-to Late Holocene East Antarctic ice-core tephrochronology: implications for reconstructing volcanic eruptions and assessing their climatic impacts over the last 5,500 years. Quat. Sci. Rev. 329, 108544. https://doi.org/10.1016/j.quascirev.2024.108544.

Abbott, P.M., Davies, S.M., 2012. Volcanism and the Greenland ice-cores: the tephra record. Earth Sci. Rev. 115, 173–191. https://doi.org/10.1016/j.earscirev.2012.09.001.

Andrews, B.J., Dufek, J., Ponomareva, V., 2018. Eruption dynamics and explosive-effusive transitions during the 1400 cal BP eruption of Opala volcano, Kamchatka, Russia. J. Volcanol. Geoth. Res. 356, 316–330. https://doi.org/10.1016/j.jvolgeores.2018.02.019.

Aubry, T.J., Engwell, S.L., Bonadonna, C., Mastin, L.G., Carazzo, G., Eaton, A.R.V., Jessop, D.E., Grainger, R.G., Scollo, S., 2023. New insights into the relationship between mass eruption rate and volcanic column height based on the IVESPA data set. Geophys. Res. Lett. 50, 1–12. https://doi.org/10.1029/2022GL102633.

Barberi, F., Coltelli, M., Frullani, A., Rosi, M., Almeida, E., 1995. Chronology and dispersal characteristics of recently (last 5000 years) erupted tephra of Cotopaxi (Ecuador): implications for long-term eruptive forecasting. J. Volcanol. Geoth. Res. 69, 217–239. https://doi.org/10.1016/0377-0273(95)00017-8.

Baroni, M., Thiemens, M.H., Delmas, R.J., Savarino, J., 2007. Mass-independent sulfur isotopic compositions in stratospheric volcanic eruptions. Science 315, 84–87. https://doi.org/10.1126/science.1131754.

Büntgen, U., Cosmo, N.D., Esper, J., Frachetti, M., Khalidi, L., Mauelshagen, F., Rohland, E., Oppenheimer, C., 2025. Volcanoes, climate, and society. Annu. Rev. Earth Planet. Sci. 54. https://doi.org/10.1146/annurev-earth-032524-013254.

Büntgen, U., Myglan, V.S., Ljungqvist, F.C., McCormick, M., Cosmo, N.D., Sigl, M., Jungclaus, J., Wagner, S., Krusic, P.J., Esper, J., Kaplan, J.O., de Vaan, M.A.C., Luterbacher, J., Wacker, L., Tegel, W., Kirdyanov, Alexander V., 2016. Cooling and societal change during the late Antique little ice age from 536 to around 660 AD. Nat. Geosci. 9, 231–237. https://doi.org/10.1038/NGEO2652.

Bolge, L.L., Carr, M.J., Feigenson, M.D., Alvarado, G.E., 2006. Geochemical stratigraphy and magmatic evolution at arenal Volcano, Costa Rica. J. Volcanol. Geoth. Res. 157, 34–48. https://doi.org/10.1016/j.jvolgeores.2006.03.036.

Bolton, M.S.M., Jensen, B.J.L., Wallace, K., Praet, N., Fortin, D., Kaufman, D., Batist, M.D.E., 2020. Machine learning classifiers for attributing tephra to source volcanoes: an evaluation of methods for Alaska tephras. J. Quat. Sci. 35, 81–92. https://doi.org/10.1002/jqs.3170.

Borchardt, G.A., Aruscava, P.J., Millard, Jr., H.T., 1972. Correlation of the Bishop Ash, a Pleistocene marker bed, using instrumental neutron activation analysis. SEPM J. Sediment. Res. 42, 301–306. https://doi.org/10.1306/74D72527-2B21-11D7-8648000102C1865D.

Bourne, A.J., Abbott, P.M., Albert, P.G., Cook, E., Pearce, N.J.G., Ponomareva, V., Svensson, A., Davies, S.M., 2016. Underestimated risks of recurrent long-range ash dispersal from northern Pacific Arc volcanoes. Sci. Rep. 6, 29837. https://doi.org/10.1038/srep29837.

Braitseva, O.A., Melekestsev, I.V., Ponomareva, V.V., Sulerzhitsky, L.D., 1995. Ages of calderas, large explosive craters and active volcanoes in the Kuril-Kamchatka region, Russia. Bull. Volcanol. 57, 383–402. https://doi.org/10.1007/BF00300984.

Braitseva, O.A., Ponomareva, V.V., Sulerzhitsky, L.D., Melekestsev, I.V., Bailey, J., 1997. Holocene key-marker tephra layers in Kamchatka, Russia. Quat. Res. 47, 125–139. https://doi.org/10.1006/qres.1996.1876.

Burke, A., Innes, H.M., Crick, L., Anchukaitis, K.J., Byrne, M.P., Hutchison, W., McConnell, J.R., Moore, K.A., Rae, J.W.B., Sigl, M., Wilson, R., 2023. High sensitivity of summer temperatures to stratospheric sulfur loading from volcanoes in the Northern Hemisphere. Proc. Natl. Acad. Sci. USA 120. https://doi.org/10.1073/pnas.2221810120.

Burke, A., Moore, K.A., Sigl, M., Nita, D.C., McConnell, J.R., Adkins, J.F., 2019. Stratospheric eruptions from tropical and extra-tropical volcanoes constrained using high-resolution sulfur isotopes in ice cores. Earth Planet Sci. Lett. 521, 113–119. https://doi.org/10.1016/j.epsl.2019.06.006.

Burke, A., Present, T.M., Paris, G., Rae, E.C.M., Sandilands, B.H., Gaillardet, J., Peuckerehrenbrink, B., Fischer, W.W., Mcclelland, J.W., Spencer, R.G.M., Voss, B.M., Adkins, J.F., 2018. Sulfur isotopes in rivers: insights into global weathering budgets , pyrite oxidation, and the modern sulfur cycle. Earth Planet Sci. Lett. 496, 168–177. https://doi.org/10.1016/j.epsl.2018.05.022.

Bursik, M., Sieh, K., Meltzner, A., 2014. Deposits of the most recent eruption in the Southern Mono Craters , California : description , interpretation and implications for regional marker tephras. J. Volcanol. Geoth. Res. 275, 114–131. https://doi.org/10.1016/j.jvolgeores.2014.02.015.

Cole, P.D., Guest, J.E., Queiroz, G., Wallenstein, N., Pacheco, J.M., Gaspar, J.L., Ferreira, T., Duncan, A.M., 1999. Styles of volcanism and volcanic hazards on Furnas volcano; Sao Miguel, Azores. J. Volcanol. Geoth. Res. 92, 39–53. https://doi.org/10.1016/S0377-0273(99)00066-9.

Cole-Dai, J., 2010. Volcanoes and climate. Clim. Change 1, 824–839. https://doi.org/10.1002/wcc.76.

Coulter, S.E., Pilcher, J.R., Plunkett, G., Baillie, M., Hall, V.A., Steffensen, J.P., Vinther, B.M., Clausen, H.B., Johnsen, S.J., 2012. Holocene tephras highlight complexity of volcanic signals in Greenland ice cores. J. Geophys. Res. 117, 1–11. https://doi.org/10.1029/2012JD017698.

Crick, L., Burke, A., Hutchison, W., Kohno, M., Moore, K.A., Savarino, J., Doyle, E.A., Mahony, S., Kipfstuhl, S., Rae, J.W.B., Steele, R.C.J., Sparks, R.S.J., Wolff, E.W., 2021. New insights into the ~ 74 ka Toba eruption from sulfur isotopes of polar ice cores. Clim. Past 17, 2119–2137. https://doi.org/10.5194/cp-17-2119-2021.

Crosweller, H.S., Arora, B., Brown, S.K., Cottrell, E., Deligne, N.I., Guerrero, N.O., Hobbs, L., Kiyosugi, K., Loughlin, S.C., Lowndes, J., Nayembil, M., Siebert, L., Sparks, R.S.J., Takarada, S., Venzke, E., 2012. Global database on large magnitude explosive volcanic eruptions (LaMEVE). J. Appl. Volcanol. 1, 4. https://doi.org/10.1186/2191-5040-1-4.

Davies, L.J., Jensen, B.J.L., Froese, D.G., Wallace, K.L., 2016. Late Pleistocene and Holocene tephrostratigraphy of interior Alaska and Yukon: key beds and chronologies over the past 30,000 years. Quat. Sci. Rev. 146, 28–53. https://doi.org/10.1016/j.quascirev.2016.05.026.

Davies, S.M., Albert, P.G., Bourne, A.J., Owen, S., Svensson, A., Bolton, M.S.M., Cook, E., Jensen, B.J.L., Jones, G., Ponomareva, V.V., 2024. Exploiting the Greenland volcanic ash repository to date caldera-forming eruptions and widespread isochrons during the Holocene. Quat. Sci. Rev. 334, 108707. https://doi.org/10.1016/j.quascirev.2024.108707.

Derkachev, A.N., Nikolaeva, N.A., Gorbarenko, S.A., Portnyagin, M.V., Ponomareva, V.V., Nürnberg, D., Sakamoto, T., Iijima, K., Liu, Y., Shi, X., Lv, H., Wang, K., 2016. Tephra layers of in the quaternary deposits of the Sea of Okhotsk: distribution, composition, age and volcanic sources. Quat. Int. 425, 248–272. https://doi.org/10.1016/j.quaint.2016.07.004.

Derkachev, A.N., Ponomareva, V.V., Portnyagin, M.V., Gorbarenko, S.A., Nikolaeva, N.A., Malakhov, M.I., Zelenin, E.A., Nürnberg, D., Liu, Y., 2018. Widespread tephra layers in the Bering Sea sediments: distal clues to large explosive eruptions from the Aleutian volcanic arc. Bull. Volcanol. 80, 1–3. https://doi.org/10.1007/s00445-018-1254-9.

Di Cosmo, N., Oppenheimer, C., Büntgen, U., 2017. Interplay of environmental and sociopolitical factors in the downfall of the Eastern Türk Empire in 630 CE. Clim. Change 145, 383–395. https://doi.org/10.1007/s10584-017-2111-0.

Ellis, B.S., Pimentel, A., Cortes-Calderon, E.A., Moser, Z., Baumann, N., Bachmann, O., Wadsworth, F.B., 2023. Obsidian clasts as sintered remnants of agglutination processes in volcanic conduits, evidence from the Pepom tephras (Sete Cidades), São Miguel, Azores. Chem. Geol. 638, 121694. https://doi.org/10.1016/j.chemgeo.2023.121694.

Endo, Y., Chen, M., Claire, M.W., 2024. An analysis of Δ36S/Δ33S dependence on definitions of sulfur mass-independent fractionation. Chem. Geol. 661, 122157. https://doi.org/10.1016/j.chemgeo.2024.122157.

Espíndola, J.M., Macías, J.L., Tilling, R.I., Sheridan, M.F., 2000. Volcanic history of El Chichón Volcano (Chiapas, Mexico) during the Holocene, and its impact on human activity. Bull. Volcanol. 62, 90–104. https://doi.org/10.1007/s004459900064.

Fabbro, G.N., Mckee, C.O., Sindang, M.E., Eggins, S., Bouvet de Maisonneuve, C., 2020. Variable mafic recharge across a caldera cycle at Rabaul, Papua New Guinea. J. Volcanol. Geoth. Res. 393, 106810. https://doi.org/10.1016/j.jvolgeores.2020.106810.

Fei, J., Zhou, J., Hou, Y., 2007. Circa A.D. 626 volcanic eruption, climatic cooling, and the collapse of the Eastern Turkic Empire. Clim. Change 81, 469–475. https://doi.org/10.1007/s10584-006-9199-y.

Firth, C., Blong, R., Haberle, S., Davies, H., Torombe, M., Coulter, S., Wagner, T., Lee, S., Singura, L., Denham, T., 2024. Holocene tephras in the New Guinea Highlands: explosive volcanism in the Bismarck arc produces chronostratigraphic markers for interdisciplinary study. Holocene 35, 234–248. https://doi.org/10.1177/09596836241297678.

Fortin, D., Praet, N., Mckay, N.P., Kaufman, D.S., Jensen, B.J.L., Haeussler, P.J., Buchanan, C., Batist, M.D., 2019. New approach to assessing age uncertainties e The 2300-year varve chronology from Eklutna Lake , Alaska (USA). Quat. Sci. Rev. 203, 90–101. https://doi.org/10.1016/j.quascirev.2018.10.018.

Gao, C., Ludlow, F., Amir, O., Kostick, C., 2016. Reconciling multiple ice-core volcanic histories: the potential of tree-ring and documentary evidence, 670-730 CE. Quat. Int. 394, 180–193. https://doi.org/10.1016/j.quaint.2015.11.098.

Gao, C., Robock, A., Ammann, C., 2008. Volcanic forcing of climate over the past 1500 years: an improved ice core-based index for climate models. J. Geophys. Res. Atmospheres 113, D23111. https://doi.org/10.1029/2008JD010239.

Gardner, J.E., Sigurdsson, H., Vulkanologie, A., 1998. Plinian eruptions at Glacier Peak and Newberry volcanoes, United States: implications for volcanic hazards in the Cascade range. GSA Bull 110, 173–187.

Garrison, J.M., Davidson, J.P., Hall, M., Mothes, P., 2011. Geochemistry and petrology of the most recent deposits from Cotopaxi Volcano, Northern volcanic zone, Ecuador. J. Petrol. 52, 1641–1678. https://doi.org/10.1093/petrology/egr023.

Gautier, E., Savarino, J., Erbland, J., Farquhar, J., 2018. SO2 oxidation kinetics leave a consistent isotopic imprint on volcanic ice core sulfate. J. Geophys. Res. Atmospheres 123, 9801–9812. https://doi.org/10.1029/2018JD028456.

Gautier, E., Savarino, J., Hoek, J., Erbland, J., Caillon, N., Hattori, S., Yoshida, N., Albalat, E., Albarede, F., Farquhar, J., 2019. 2600-years of stratospheric volcanism through sulfate isotopes. Nat. Commun. 10, 1–7. https://doi.org/10.1038/s41467-019-08357-0.

Geshi, N., Oikawa, T., Weller, D.J., Conway, C.E., 2022. Evolution of the magma plumbing system of Miyakejima volcano with periodic recharge of basaltic magmas. Earth Planets Space 74. https://doi.org/10.1186/s40623-022-01577-7.

Hall, M., Mothes, P., 2008. The rhyolitic-andesitic eruptive history of Cotopaxi volcano, Ecuador. Bull. Volcanol. 70, 675–702. https://doi.org/10.1007/s00445-007-0161-2.

Hayward, C., 2012. High spatial resolution electron probe microanalysis of tephras and melt inclusions without beam-induced chemical modification. Holocene 22, 119–125. https://doi.org/10.1177/0959683611409777.

Hutchison, W., Gabriel, I., Plunkett, G., Burke, A., Sugden, P., Innes, H., Davies, S., Moreland, W.M., Krüger, K., Wilson, R., Vinther, B.M., Dahl-Jensen, D., Freitag, J., Oppenheimer, C., Chellman, N.J., Sigl, M., McConnell, J.R., 2024. High-resolution ice-core analyses identify the eldgjá eruption and a cluster of Icelandic and transcontinental tephras between 936 and 943 CE. J. Geophys. Res. Atmospheres 129, 1–21. https://doi.org/10.1029/2023JD040142.

Hutchison, W., Sugden, P., Burke, A., Abbott, P.M., Ponomareva, V.V., Dirksen, O., Portnyagin, M.V., MacInnes, B., Bourgeois, J., Fitzhugh, B., Verkerk, M., Aubry, T.J., Engwell, S.L., Svensson, A., Chellman, N.J., McConnell, J.R., Davies, S.M., Sigl, M., Plunkett, G., 2025. The 1831 CE mystery eruption identified as Zavaritskii caldera, Simushir Island (Kurils). Proc. Natl. Acad. Sci. USA 122, e2316699122. https://doi.org/10.1073/pnas.2416699122.

Innes, H.M., Hutchison, W., Burke, A., 2024. Geochemical analysis of extremely fine-grained cryptotephra: new developments and recommended practices. Quat. Geochronol. 83, 101553. https://doi.org/10.1016/j.quageo.2024.101553.

Iverson, N.A., Kalteyer, D., Dunbar, N.W., Kurbatov, A., Yates, M., 2017. Advancements and best practices for analysis and correlation of tephra and cryptotephra in ice. Quat. Geochronol. 40, 45–55. https://doi.org/10.1016/j.quageo.2016.09.008.

Jensen, B.J.L., Davies, L.J., Nolan, C., Donnell, S.P., Monteath, A.J., Ponomareva, V., Portnyagin, M., Booth, R., Bursik, M., Cook, E., Plunkett, G., Vallance, J.W., Luo, Y., Cwynar, L.C., Hughes, P., Pearson, D.G., 2021. A latest Pleistocene and Holocene composite tephrostratigraphic framework for northeastern North America. Quat. Sci. Rev. 272, 107242. https://doi.org/10.1016/j.quascirev.2021.107242.

Jensen, B.J.L., Pyne-O'Donnell, S., Plunkett, G., Froese, D.G., Hughes, P.D.M., Sigl, M., McConnell, J.R., Amesbury, M.J., Blackwell, P.G., van den Bogaard, C., Buck, C.E., Charman, D.J., Clague, J.J., Hall, V.A., Koch, J., Mackay, H., Mallon, G., McColl, L., Pilcher, J.R., 2014. Transatlantic distribution of the Alaskan White River Ash. Geology 42 (1), 875–878. https://doi.org/10.1130/G35945.

Jochum, K.P., Stoll, B., Herwig, K., Willbold, M., Hofmann, A.W., Amini, M., Aarburg, S., Abouchami, W., Hellebrand, E., Mocek, B., Raczek, I., Stracke, A., Alard, O., Bouman, C., Becker, S., Dücking, M., Brätz, H., Klemd, R., De Bruin, D., Canil, D., Cornell, D., De Hoog, C.J., Dalpé, C., Danyushevshy, L., Eisenhauer, A., Gao, Y., Snow, J.E., Groschopf, N., Günther, D., Latkoczy, C., Guillong, M., Hauri, E.H., Höfer, H.E., Lahaye, Y., Horz, K., Jacob, D.E., Kasemann, S.A., Kent, A.J.R., Ludwig, T., Zack, T., Mason, P.R.D., Meixner, A., Rosner, M., Misawa, K., Nash, B.P., Pfänder, J., Premo, W.R., Sun, W.D., Tiepolo, M., Vannucci, R., Vennemann, T., Wayne, D., Woodhead, J.D., 2006. MPI-DING reference glasses for in situ microanalysis: new reference values for element concentrations and isotope ratios. Geochem. Geophys. Geosystems 7, Q02008. https://doi.org/10.1029/2005GC001060.

Jochum, K.P., Weis, U., Stoll, B., Kuzmin, D., Yang, Q., Raczek, I., Jacob, D.E., Stracke, A., Birbaum, K., Frick, D.A., Günther, D., Enzweiler, J., 2011. Determination of reference values for NIST SRM 610-617 glasses following ISO guidelines. Geostand. Geoanalytical Res. 35, 397–429. https://doi.org/10.1111/j.1751-908X.2011.00120.x.

Jongebloed, U.A., Schauer, A.J., Cole-Dai, J., Larrick, C.G., Wood, R., Fischer, T.P., Carn, S.A., Salimi, S., Edouard, S.R., Zhai, S., Geng, L., Alexander, B., 2023. Underestimated passive volcanic sulfur degassing implies overestimated anthropogenic aerosol forcing. Geophys. Res. Lett. 50, 12. https://doi.org/10.1029/2022GL102061.

Jungclaus, J.H., Bard, E., Baroni, M., Braconnot, P., Cao, J., Chini, L.P., Egorova, T., Evans, M., Fidel González-Rouco, J., Goosse, H., Hurtt, G.C., Joos, F., Kaplan, J.O., Khodri, M., Klein Goldewijk, K., Krivova, N., Legrande, A.N., Lorenz, S.J., Luterbacher, J., Man, W., Maycock, A.C., Meinshausen, M., Moberg, A., Muscheler, R., Nehrbass-Ahles, C., Otto-Bliesner, B.I., Phipps, S.J., Pongratz, J., Rozanov, E., Schmidt, G.A., Schmidt, H., Schmutz, W., Schurer, A., Shapiro, A.I., Sigl, M., Smerdon, J.E., Solanki, S.K., Timmreck, C., Toohey, M., Usoskin, I.G., Wagner, S., Wu, C.J., Leng Yeo, K., Zanchettin, D., Zhang, Q., Zorita, E., 2017. The PMIP4 contribution to CMIP6 - part 3: the last millennium, scientific objective, and experimental design for the PMIP4 past1000 simulations. Geosci. Model Dev. 10, 4005–4033. https://doi.org/10.5194/gmd-10-4005-2017.

Krasheninnikov, S.P., Bazanova, L.I., Ponomareva, V.V., Portnyagin, M.V., 2020. Detailed tephrochronology and composition of major Holocene eruptions from Avachinsky, Kozelsky, and Koryaksky volcanoes in Kamchatka. J. Volcanol. Geoth. Res. 408, 107088. https://doi.org/10.1016/j.jvolgeores.2020.107088.

Kuehn, S.C., 2002. Stratigraphy, Distribution, and Geochemistry of the Newberry Volcano Tephras. State Univ. PhD Thesis Wash.

Kuehn, S., Froese, D.G., Pearce, N.J.G., Foit, F.F., 2009. ID3506, a new/old lipari Obsidian standard for characterization of natural glasses and for tephrochronology. In: 2009 AGU Fall Meeting. https://doi.org/10.13140/RG.2.1.1834.9282.

Kuehn, S.C., Froese, D.G., Shane, P.A.R., Participants, I.I., 2011. The INTAV intercomparison of electron-beam microanalysis of glass by tephrochronology laboratories: results and recommendations. Quat. Int. 246, 19–47. https://doi.org/10.1016/j.quaint.2011.08.022.

Kuehn, S.C., Foit, F.F., 2006. Correlation of widespread Holocene and Pleistocene tephra layers from newberry Volcano, Oregon, USA, using glass compositions and numerical analysis. Quat. Geochronol. 148, 113–137. https://doi.org/10.1016/j.quaint.2005.11.008.

Lowe, D.J., 2011. Tephrochronology and its application: a review. Quat. Geochronol. 6, 107–153. https://doi.org/10.1016/j.quageo.2010.08.003.

Lubbers, J., Loewen, M., Wallace, K., Coombs, M., Addison, J., 2023. Probabilistic source classification of large tephra producing eruptions using supervised machine learning: an example from the alaska-aleutian arc. Geochem. Geophys. Geosystems 24. https://doi.org/10.1029/2023GC011037.

Mackay, H., Plunkett, G., Jensen, B.J.L., Aubry, T.J., Corona, C., Kim, W.M., Toohey, M., Sigl, M., Stoffel, M., Anchukaitis, K.J., Raible, C., Bolton, M.S.M., Manning, J.G., Newfield, T.P., Di Cosmo, N., Ludlow, F., Kostick, C., Yang, Z., Coyle Mcclung, L., Amesbury, M., Monteath, A., Hughes, P.D.M., Langdon, P.G., Charman, D., Booth, R., Davies, K.L., Blundell, A., Swindles, G.T., 2022. The 852/3 CE Mount Churchill eruption: examining the potential climatic and societal impacts and the timing of the Medieval Climate anomaly in the North Atlantic region. Clim. Past 18, 1475–1508. https://doi.org/10.5194/cp-18-1475-2022.

Marshall, L., Johnson, J.S., Mann, G.W., Lee, L., Dhomse, S.S., Regayre, L., Yoshioka, M., Carslaw, K.S., Schmidt, A., 2019. Exploring how eruption source parameters affect volcanic radiative forcing using statistical emulation. J. Geophys. Res. Atmospheres 124, 964–985. https://doi.org/10.1029/2018JD028675.

Marshall, L.R., Maters, E.C., Schmidt, A., Timmreck, C., Robock, A., Toohey, M., Marshall, L.R., 2022. Volcanic effects on climate: recent advances and future avenues. Bull. Volcanol. 84. https://doi.org/10.1007/s00445-022-01559-3.

Maruyama, S., Hattori, K., Hirata, T., Suzuki, T., Danhara, T., 2016. Simultaneous determination of 58 major and trace elements in volcanic glass shards from the INTAV sample mount using femtosecond laser ablation-inductively coupled plasma-mass spectrometry. Geochem. J. 50, 403–422. https://doi.org/10.2343/geochemj.2.0436.

McConnell, J.R., Chellman, N.J., Plach, A., Wensman, S.M., Plunkett, G., Stohl, A., Smith, N.-K., Vinther, B.M., Dahl-Jensen, D., Steffensen, J.P., Fritzsche, D., Camara-Brugger, S.O., McDonald, B.T., Wilson, A.I., 2025. European atmospheric lead pollution, enhanced blood lead levels, and cognitive decline from Roman–era mining and smelting. Proc. Natl. Acad. Sci. USA 122, e2419630121. https://doi.org/10.1073/pnas.

McConnell, J.R., Lamorey, G.W., Lambert, S.W., Taylor, K.C., 2002. Continuous ice-core chemical analyses using inductively coupled plasma mass spectrometry. Environ. Sci. Technol. 36, 7–11. https://doi.org/10.1021/es011088z.

McConnell, J.R., Sigl, M., Plunkett, G., Burke, A., Kim, W.M., Raible, C.C., Wilson, A.I., Manning, J.G., Ludlow, F., Chellman, N.J., Innes, H.M., Yang, Z., Larsen, J.F., Schaefer, J.R., Kipfstuhl, S., Mojtabavi, S., Wilhelms, F., Opel, T., Meyer, H., Steffensen, J.P., 2020. Extreme climate after massive eruption of Alaska's Okmok volcano in 43 BCE and effects on the late Roman Republic and Ptolemaic kingdom. Proc. Natl. Acad. Sci. USA 117, 15443–15449. https://doi.org/10.1073/pnas.2002722117.

McKee, C.O., Baillie, M.G., Reimer, P.J., 2015. A revised age of AD 667–699 for the latest major eruption at Rabaul. Bull. Volcanol. 77, 1–7. https://doi.org/10.1007/s00445-015-0954-7.

McKee, C.O., Neall, V.E., Torrence, R., 2011. A remarkable pulse of large-scale volcanism on New Britain Island, Papua New Guinea. Bull. Volcanol. 73, 27–37. https://doi.org/10.1007/s00445-010-0401-8.

Moore, R.B., Rubin, M., 1991. Radiocarbon dates for lava flows and pyroclastic deposits on São Miguel, azores. Radiocarbon 33, 151–164. https://doi.org/10.1017/S0033822200013278.

Nathenson, M., 2017. Revised tephra volumes for Cascade Range volcanoes. J. Volcanol. Geoth. Res. 341, 42–52. https://doi.org/10.1016/j.jvolgeores.2017.04.021.

Neall, V., McGee, L., Turner, M., O'Neill, T., Zernack, A., Athens, J.S., 2021. Geochemical fingerprinting of Holocene tephras in the willaumez isthmus district of West New Britain, Papua New Guinea. Tech. Rep. Aust. Mus. Online 34, 5–24. https://doi.org/10.3853/j.1835-4211.34.2021.1740.

Nooren, K., Hoek, W.Z., van der Plicht, H., Sigl, M., van Bergen, M.J., Galop, D., Torrescano-Valle, N., Islebe, G., Huizinga, A., Winkels, T., Middelkoop, H., 2017. Explosive eruption of El Chichon volcano (Mexico) disrupted 6th century Maya civilization and contributed to global cooling. Geology 45 (1), 175–178. https://doi.org/10.1130/G38739.

PAGES 2k Consortium, 2013. Continental-scale temperature variability during the past two millennia. Nat. Geosci. 6, 339–346. https://doi.org/10.1038/ngeo1797.

Paton, C., Hellstrom, J., Paul, B., Woodhead, J., Hergt, J., 2011. Iolite: freeware for the visualisation and processing of mass spectrometric data. J. Anal. At. Spectrom. 26, 2508–2518. https://doi.org/10.1039/c1ja10172b.

Pearson, C., Sigl, M., Burke, A., Davies, S., Kurbatov, A., Severi, M., Cole-Dai, J., Innes, H., Albert, P.G., Helmick, M., 2022. Geochemical ice-core constraints on the timing and climatic impact of Aniakchak II (1628 BCE) and Thera (Minoan) volcanic eruptions. PNAS Nexus 1, 1–12. https://doi.org/10.1093/pnasnexus/pgac048.

Plunkett, G., Coulter, S.E., Ponomareva, V.V., Blaauw, M., Klimaschewski, A., Hammarlund, D., 2015. Distal tephrochronology in volcanic regions: challenges and insights from Kamchatkan lake sediments. Glob. Planet. Change 134, 26–40. https://doi.org/10.1016/j.gloplacha.2015.04.006.

Plunkett, G., Sigl, M., McConnell, J.R., Pilcher, J.R., Chellman, N.J., 2023. The significance of volcanic ash in Greenland ice cores during the Common era. Quat. Sci. Rev. 301, 107936. https://doi.org/10.1016/j.quascirev.2022.107936.

Plunkett, G., Sigl, M., Schwaiger, H.F., Tomlinson, E.L., Toohey, M., Mcconnell, J.R., Pilcher, J.R., Hasegawa, T., Siebe, C., 2022. No evidence for tephra in Greenland from the historic eruption of Vesuvius in 79 CE: implications for geochronology and paleoclimatology. Clim. Past 18, 45–65. https://doi.org/10.5194/cp-18-45-2022.

Ponomareva, V., Portnyagin, M., Davies, S.M., 2015. Tephra without borders: Far-reaching clues into past explosive eruptions. Front. Earth Sci. 3. https://doi.org/10.3389/feart.2015.00083.

Ponomareva, V., Portnyagin, M., Pendea, I.F., Zelenin, E., Bourgeois, J., Pinegina, T., Kozhurin, A., 2017. A full holocene tephrochronology for the Kamchatsky Peninsula region: applications from Kamchatka to North America. Quat. Sci. Rev. 168, 101–122. https://doi.org/10.1016/j.quascirev.2017.04.031.

Portnyagin, M.V., Ponomareva, V.V., Zelenin, E.A., Bazanova, L.I., Pevzner, M.M., Plechova, A.A., Rogozin, A.N., Garbe-Schönberg, Di, 2020. TephraKam: geochemical database of glass compositions in tephra and welded tuffs from the Kamchatka volcanic arc (northwestern Pacific). Earth Syst. Sci. Data 12, 469–486. https://doi.org/10.5194/essd-12-469-2020.

Praet, N., van Daele, M., Moernaut, J., Mestdagh, T., Vandorpe, T., Jensen, B.J.L., Witter, R.C., Haeussler, P.J., Batist, M.D., 2022. Unravelling a 2300 year long sedimentary record of megathrust and intraslab earthquakes in proglacial Skilak Lake, south-central Alaska. Sedimentology 69, 2151–2180. https://doi.org/10.1111/sed.12986.

Putnam, W.C., 1938. The Mono craters, California. Geogr. Rev. 28, 68. https://doi.org/10.2307/210567.

Pyne-O'Donnell, S.D.F., Hughes, P.D.M., Froese, D.G., Jensen, B.J.L., Kuehn, S.C., Mallon, G., Amesbury, M.J., Charman, D.J., Daley, T.J., Loader, N.J., Mauquoy, D., Street-Perrott, F.A., Woodman-Ralph, J., 2012. High-precision ultra-distal Holocene tephrochronology in North America. Quat. Sci. Rev. 52, 6–11. https://doi.org/10.1016/j.quascirev.2012.07.024.

Queiroz, G., Gaspar, J.L., Guest, J.E., Gomes, A., Almeida, M.H., 2015. Chapter 7 eruptive history and evolution of Sete Cidades Volcano, Sao Miguel Island, Azores. Volcan. Geol. Sao Miguel Isl. Azores Archipel. Geol. Soc. Lond. Mem. 44, 87–104.

Queiroz, G., Pacheco, J.M., Gaspar, J.L., Aspinall, W.P., Guest, J.E., Ferreira, T., 2008. The last 5000 years of activity at Sete Cidades volcano (São Miguel Island, Azores): implications for hazard assessment. J. Volcanol. Geoth. Res. 178, 562–573. https://doi.org/10.1016/j.jvolgeores.2008.03.001.

Riehle, J.R., 1985. A reconnaissance of the major Holocene tephra deposits in the upper Cook Inlet region, Alaska. J. Volcanol. Geoth. Res. 26, 37–74.

Robock, A., 2000. Volcanic eruptions and climate. Rev. Geophys. 38, 191–219. https://doi.org/10.1029/1998RG000054.

Rust, A.C., Cashman, K.V., 2007. Multiple origins of obsidian pyroclasts and implications for changes in the dynamics of the 1300 B.P. eruption of Newberry Volcano, USA. Bull. Volcanol. 69, 825–845. https://doi.org/10.1007/s00445-006-0111-4.

Salzer, M.W., Hughes, M.K., 2007. Bristlecone pine tree rings and volcanic eruptions over the last 5000 yr. Quarternary Res 67, 57–68. https://doi.org/10.1016/j.yqres.2006.07.004.

Salzer, M.W., Kipfmueller, K.F., 2005. Reconstructed temperature and precipitation on a millennial timescale from tree-rings in the southern Colorado Plateau. USA Clim. Change 70, 465–487. https://doi.org/10.1007/s10584-005-5922-3.

Savarino, J., Romero, A., Cole-Dai, J., Bekki, S., Thiemens, M.H., 2003. UV induced mass-independent sulfur isotope fractionation in stratospheric volcanic sulfate. Geophys. Res. Lett. 30, 2131. https://doi.org/10.1029/2003GL018134.

Schindlbeck, J.C., Kutterolf, S., Straub, S.M., Andrews, G.D.M., Wang, K., Mleneck-Vautravers, M.J., 2017. One Million Years tephra record at IODP Sites U1436 and U1437: insights into explosive volcanism from the Japan and Izu arcs. Isl. Arc 27, e12244. https://doi.org/10.1111/iar.12244.

Schneider, L., Smerdon, J.E., Büntgen, U., Wilson, R.J.S., Myglan, V.S., Kirdyanov, A.V., Esper, J., 2015. Revising midlatitude summer temperatures back to A.D. 600 based on a wood density network. Geophys. Res. Lett. 42, 4556–4562. https://doi.org/10.1002/2015GL063956.

Sieh, K., Bursik, M., 1986. Most recent eruption of the Mono Craters, eastern central California. J. Geophys. Res. Solid Earth 91, 12539–12571. https://doi.org/10.1029/JB091iB12p12539.

Sigl, M., Toohey, M., McConnell, J.R., Cole-dai, J., Severi, M., 2022. Volcanic stratospheric sulfur injections and aerosol optical depth during the Holocene (past 11 500 years) from a bipolar ice-core array. Earth Syst. Sci. Data 14, 3167–3196. https://doi.org/10.5194/essd-14-3167-2022.

Sigl, M., Winstrup, M., McConnell, J.R., Welten, K.C., Plunkett, G., Ludlow, F., Büntgen, U., Caffee, M., Chellman, N., Dahl-Jensen, D., Fischer, H., Kipfstuhl, S., Kostick, C., Maselli, O.J., Mekhaldi, F., Mulvaney, R., Muscheler, R., Pasteris, D.R., Pilcher, J.R., Salzer, M., Schüpbach, S., Steffensen, J.P., Vinther, B.M., Woodruff, T.E., 2015. Timing and climate forcing of volcanic eruptions for the past 2,500 years. Nature 523, 543–549. https://doi.org/10.1038/nature14565.

Smith, V.C., Costa, A., Aguirre-Díaz, G., Pedrazzi, D., Scifo, A., Plunkett, G., Poret, M., Tournigand, P.Y., Miles, D., Dee, M.W., McConnell, J.R., Sunyé-Puchol, I., Harris, P.D., Sigl, M., Pilcher, J.R., Chellman, N., Gutiérrez, E., 2020. The magnitude and impact of the 431 CE Tierra Blanca Joven eruption of Ilopango, El Salvador. Proc. Natl. Acad. Sci. USA 117, 26061–26068. https://doi.org/10.1073/pnas.2003008117.

Stevenson, S., Fasullo, J.T., Otto-Bliesner, B.L., Tomas, R.A., Gao, C., 2017. Role of eruption season in reconciling model and proxy responses to tropical volcanism. Proc. Natl. Acad. Sci. USA 114, 1822–1826. https://doi.org/10.1073/pnas.1612505114.

Stothers, R.B., 2002. Cloudy and clear stratospheres before A.D. 1000 inferred from written sources. J. Geophys. Res. 107 (D23). https://doi.org/10.1029/2002JD002105. AAC-17.

Stothers, R.B., Rampino, M.R., 1983. Volcanic eruptions in the Mediterranean before A.D. 630 from written and archaeological sources. J. Geophys. Res. 88, 6357–6371. https://doi.org/10.1029/JB088iB08p06357.

Sun, S.S., McDonough, W.F., 1989. Chemical and isotopic systematics of oceanic basalts: implications for mantle composition and processes. Geol. Soc. Spec. Publ. 42, 313–345. https://doi.org/10.1144/GSL.SP.1989.042.01.19.

Tomlinson, E.L., Smith, V.C., Albert, P.G., Aydar, E., Civetta, L., Cioni, R., Çubukçu, E., Gertisser, R., Isaia, R., Menzies, M.A., Orsi, G., Rosi, M., Zanchetta, G., 2015. The major and trace element glass compositions of the productive Mediterranean volcanic sources: tools for correlating distal tephra layers in and around Europe. Quat. Sci. Rev. 118, 48–66. https://doi.org/10.1016/j.quascirev.2014.10.028.

Toohey, M., Krüger, K., Niemeier, U., Timmreck, C., 2011. The influence of eruption season on the global aerosol evolution and radiative impact of tropical volcanic eruptions. Atmos. Chem. Phys. 11, 12351–12367. https://doi.org/10.5194/acp-11-12351-2011.

Toohey, M., Krüger, K., Schmidt, H., Timmreck, C., Sigl, M., Stoffel, M., Wilson, R., 2019. Disproportionately strong climate forcing from extratropical explosive volcanic eruptions. Nat. Geosci. 12, 100–107. https://doi.org/10.1038/s41561-018-0286-2.

Toohey, M., Sigl, M., 2017. Volcanic stratospheric sulfur injections and aerosol optical depth from 500 BCE to 1900 CE. Earth Syst. Sci. Data 9, 809–831. https://doi.org/10.5194/essd-9-809-2017.

Wang, L., Roucoux, K.H., Davies, A.L., Zhang, S., Sun, C., Streeter, R.T., Hutchison, W., Lawson, I.T., 2025. A new tephrochronological record of a raised bog in eastern lowland Scotland. Quat. Geochronol. 86, 101647. https://doi.org/10.1016/j.quageo.2024.101647.

Wastegård, S., Johansson, H., Pacheco, J.M., 2020. New major element analyses of proximal tephras from the Azores and suggested correlations with cryptotephras in North-West Europe. J. Quat. Sci. 35, 114–121. https://doi.org/10.1002/jqs.3155.

Watson, E.J., Swindles, G.T., Savov, I.P., Lawson, I.T., Connor, C.B., Wilson, J.A., 2017. Estimating the frequency of volcanic ash clouds over northern Europe. Earth Planet Sci. Lett. 460. https://doi.org/10.1016/j.epsl.2016.11.054.

Zielinski, G.A., Mayewski, P.A., Meeker, L.D., Whitlow, S., Twickler, M.S., Morrison, M., Meese, D.A., Gow, A.J., Alley, R.B., 1994. Record of volcanism since 7000 B.C. from the GISP2 Greenland ice core and implications for the volcano-climate System. Science 264, 948–952. https://doi.org/10.1126/science.264.5161.948.